A Uniform Analysis of 118 Stars with High-Contrast Imaging: Long Period Extrasolar Giant Planets are Rare around Sun-like Stars

Eric L. Nielsen[1] and Laird M. Close

Steward Observatory, University of Arizona, Tucson, AZ 85721

enielsen@as.arizona.edu

Received _____; accepted _____

[1]Michelson Fellow

ABSTRACT

We expand on the results of Nielsen et al. (2008), using the null result for giant extrasolar planets around the 118 target stars from the VLT NACO H and Ks band planet search (Masciadri et al. 2005), the VLT and MMT Simultaneous Differential Imaging (SDI) survey (Biller et al. 2007), and the Gemini Deep Planet Survey (Lafrenière et al. 2007) to set constraints on the population of giant extrasolar planets. Our analysis is extended to include the planet luminosity models of Fortney et al. (2008), as well as the correlation between stellar mass and frequency of giant planets found by Johnson et al. (2007). Doubling the sample size of FGKM stars strengthens our conclusions: a model for extrasolar giant planets with power-laws for mass and semi-major axis as giving by Cumming et al. (2008) cannot, with 95% confidence, have planets beyond 65 AU, compared to the value of 94 AU reported in Nielsen et al. (2008), using the models of Baraffe et al. (2003). When the Johnson et al. (2007) correction for stellar mass (which gives fewer Jupiter-mass companions to M stars with respect to solar-type stars) is applied, however, this limit moves out to 82 AU. For the relatively new Fortney et al. (2008) models, which predict fainter planets across most of parameter space, these upper limits, with and without a correction for stellar mass, are 182 and 234 AU, respectively.

Subject headings: stars: planetary systems

1. Introduction

There are currently close to 300 extrasolar planets known, most detected by the radial velocity method (Butler et al. 2006). These planets have provided a great deal of information on the distribution of giant planets in short period orbits. The likelihood of a star harboring a close-in giant planet increases with the metal abundance of the parent star (Fischer & Valenti 2005; Santos et al. 2004), and power laws were found to accurately represent the distributions of mass and semi-major axis of exoplanets (Cumming et al. 2008). While radial velocity surveys have moved on to discovering and building up statistics on smaller Neptune-mass planets, direct imaging surveys continue to struggle to reach even the highest mass planets.

Many observing campaigns have been conducted in the last decade to detect and characterize planets through direct imaging, especially aimed at young target stars, when the self-luminosity of hosted planets is large enough to overcome the glare of the parent star. Improvements in adaptive optics and instrumentation designed solely to detect planets, as well as specialized observing techniques, have improved the contrasts achievable close to the target star. This has allowed a large increase in sensitivity to planets, and resulted in the discovery of several planetary-mass ($<$13 M_{Jup}) objects, including companions to 2MASS 1207-3932 (Chauvin et al. 2004), HIP 30034 (AB Pic) (Chauvin et al. 2005), Oph 1622 (Close et al. 2007; Brandeker et al. 2006; Luhman et al. 2007a), and DH Tau (Itoh et al. 2005). These objects were discovered with projected separations of 42, 260, 243, and 330 AU, respectively. Few, if any, of these wide companions ($>$200 AU for objects found around stars) are likely to have formed in the primordial circumstellar disk of the primary.

Recently there have been exciting discoveries of planetary-mass objects around the higher-mass A stars: HR 8799, Fomalhaut, and β Pic (Marois et al. 2008; Kalas et al. 2008; Lagrange et al. 2009). In the case of the triple planet system HR 8799, we know that the

largest separation planet (HR 8799 b, with a projected separation of 68 AU) has the same parallax as the primary (Close & Males 2009) and so it (and very likely HR 8799 c and d) formed together around the A5 star HR 8799. While this is an amazing system, in this study we concentrate on lower mass stars, more similar to the Sun.

In Nielsen et al. (2008), we presented null results from the direct imaging surveys for extrasolar giant planets of Masciadri et al. (2005) and Biller et al. (2007), using the contrast curves for each of 60 unique target stars to set constraints on the populations of extrasolar planets. We concluded that extrasolar giant planets are rare at large separations (>60 AU). Just prior to the publication of our work, Lafrenière et al. (2007) published the null results from the Gemini Deep Planet Survey (GDPS) for 85 stars, reaching conclusions very similar to ours. In this paper, we combine the samples from these three surveys, to improve the statistical constraints we can place on extrasolar giant planet populations.

Also since these past publications, two important papers have been published relevant to direct imaging of extrasolar giant planets. Johnson et al. (2007) compared radial velocity target stars of different masses, and found that less massive stars have a lower likelihood of hosting a giant planet (>0.8 M_{Jup}). Since direct imaging surveys lean heavily on the M stars in their samples (as these are intrinsically fainter, making the detection of close-in planets easier), we attempt here to estimate the corresponding decrease in the strength of earlier null results. Also, a new set of planet luminosity models have been published by Fortney et al. (2008), which differ from the popular "hot start" models of Burrows et al. (2003) and Baraffe et al. (2003) which had been previously utilized in such work. These new models are based heavily on the "core accretion" model of planet formation, and tend to predict consistently fainter fluxes for giant planets, especially at the youngest ages and largest planet masses. In addition to significantly enlarging the sample, this paper takes into account the stellar mass dependence of planet frequency, and the new core accretion

models of Fortney et al. (2008), to present more realistic constraints on the distribution of extrasolar giant planets around Sun-like stars.

2. Observations

2.1. VLT NACO H and Ks imaging

Masciadri et al. (2005) carried out a survey of 28 young, nearby, late-type stars with the NACO adaptive optics system at the 8.2 meter Very Large Telescope (VLT). These observations have exposure times of order 30 minutes, with stars being observed in the H or Ks bands. For the 22 stars used (see Section 2.4) from the VLT NACO survey of Masciadri et al. (2005), the median target star is a 12 Myr old K7 star at 30 pc.

2.2. VLT NACO and MMT SDI

A survey of 54 young, nearby stars of a variety of spectral types (between A and M) was conducted between 2003 and 2005, with the results reported in Biller et al. (2007). This second survey used the Simultaneous Differential Imager (SDI) at the 6.5 meter MMT and the 8 meter VLT, an adaptive optics observational mode that allows higher contrasts by imaging simultaneously in narrow wavelength regions surrounding the 1.6 μm methane feature seen in cool brown dwarfs and expected in extrasolar planets (Lenzen et al. 2004; Close et al. 2005) (Swain et al. (2008) have recently detected methane in the atmosphere of the transiting extrasolar planet HD 189733b). This allows the light from a hypothetical companion planet to be more easily distinguishable from the speckle noise floor (uncorrected starlight), as the two will have very different spectral signatures in this region. This translates to higher sensitivity at smaller separations than the observations of Masciadri et al. (2005), which were conducted before the VLT SDI device was commissioned

(see Fig. 14 of Biller et al. (2007) for a more detailed comparison of the two surveys). For most of these SDI targets, the star was observed for a total of 40 minutes of integration time, which includes a 33 degree roll in the telescope's rotation angle, in order to separate super speckles–which are created within the instrument, and so will not rotate–from a physical companion, which will rotate on the sky (Biller et al. 2006). The 50 stars used from the Biller et al. (2007) SDI survey have a median age, distance, and spectral type of 70 Myr, 24 pc, and K1, respectively.

2.3. Gemini Deep Planet Survey

At about the same time as the Biller et al. (2007) SDI survey, a direct imaging campaign was underway from the Gemini North telescope using the Altair AO system and NIRI camera, imaging in a narrow-band H filter with transmission between 1.54-1.65 μm. The observations were done using the Angular Differential Imaging (ADI) technique, which leaves the Cassegrain instrument rotator off during a sequence of exposures on the star, so that instrumental effects like super speckles will stay fixed, while physical companions (like planets) will rotate throughout the observation (Liu 2004; Marois et al. 2006; Lafrenière et al. 2007). This technique is most effective at producing high contrasts as one moves away from the star, with the contrasts achieved exceeding those with SDI (Biller et al. 2007) beyond $\sim$0.7". For the 71 of the 85 stars from the GDPS survey of Lafrenière et al. (2007) which we consider here, the median target star is a K0 star at a distance of 22 pc, with an age of 248 Myr. Hence, the target stars of this survey are somewhat closer and older, whereas the southern VLT SDI survey was focused on more distant, though younger, stars.

2.4. Target Stars

Between the three surveys listed above, our analysis considers 118 distinct target stars, with some overlap between surveys. General properties of the target stars, including name, position, distance, spectral type, age, fluxes, and observation method are given in Table 1. We attempt to derive ages in a uniform manner for all target stars, using the same method as in Nielsen et al. (2008). If the star is a member of a known moving group, the age of that group is adopted as the age of the star. We limit moving group identifications to the well-studied and established groups AB Dor, Her/Lyr, Tuc/Hor, β Pic, and TW Hya. Membership in more controversial associations, such as the Local Association and IC 2391 (e.g. Fernández et al. (2008)), are not adopted here. If the star is not a member of a group, but has a measured value of the calcium emission indicator R'$_{HK}$ and a measurement of the equivalent width of the lithium absorption at 6708 $\AA$, the average of the ages from the two methods is used. If only one of these two spectral age indicators is available, the age from that measurement is used. If a star from any of the three surveys has none of these three sources for an age estimate, it is simply not used in this work. As a result, 6 stars from the Masciadri et al. (2005) survey, 1 star from the Biller et al. (2007) survey, and 14 stars from the Lafrenière et al. (2007) survey were dropped.

In order to determine ages from the R'$_{HK}$ value, we utilize the polynomial fit derived by Mamajek & Hillenbrand (2008). The authors derive their relation from R'$_{HK}$ values of young clusters, and find a precision of 0.2 dex for ages derived from this relation.

For lithium values, we compare the equivalent width of the 6707 $\AA$ lithium line and effective temperature of the star to a set of young stellar clusters. For each cluster (NGC 2264 - 3 Myr (Soderblom et al. 1999), IC 2602 - 50 Myr (Randich et al. 2001), Pleiades - 125 Myr (Soderblom et al. 1993a), M34 - 250 Myr (Jones et al. 1997), Ursa Majoris - 300 Myr (Soderblom et al. 1993b), M67 - 5200 Myr (Jones et al. 1999)), the mean lithium

equivalent width is fit as a function of effective temperature. Then, for our target stars, we interpolate between the fits to each cluster for that star's effective temperature, and the lithium value gives us the age (E. Mamajek private communication).

For target stars with both a lithium and an R'$_{HK}$ age measurement, the median scatter between the two is a factor of 3. When we consider stars in our target list that belong to a single moving group (e.g. AB Dor or β Pic), and compute their ages using only the lithium or R'$_{HK}$ method (that is, we temporarily ignore their membership in a group), we find the scatter in the computed age, between members of the same moving group, to also be about a factor of 3. This suggests that the noise in our age measurements is primarily astrophysical in nature. While finding a precise age for any single target star is notoriously difficult, our hope is that by using a large sample of stars the individual errors will average out of our final results.

Table 2 gives details on measurements (if available) for each of the three age determination methods used here, as well as the final adopted age, for each target star. We also plot our targets in Fig. 1, giving the age, distance, and spectral type (using absolute H magnitude as a proxy) for each star. Overall, for all 118 of the stars considered in this paper, the median target star is a K1 star at a distance of 24 pc with an age of 160 Myr.

3. Monte Carlo Simulations

As in Nielsen et al. (2008) we use Monte Carlo simulations of "fake" planets around each of the target stars in the three direct imaging surveys considered here. A large number (10^4 - 10^5, depending on the application) of simulated planets are given random values of eccentricity, viewing angles, and orbital phase based on the appropriate distributions. Planet mass and semi-major axis are assigned either from a grid (see Section 3.3), or

from power-law distributions (as in Section 3.4). For graphical representations of the distributions of extrasolar planet orbital parameters, see Fig. 2, 5, and 6 of Nielsen et al. (2008), and the discussion therein. For each observation of a given target star, the flux of each simulated planet is computed based on the planet's mass and the target star's age, using one of three planet models (see Section 3.1). The angular separation between parent star and simulated planet, as well as the flux ratio between planet and star, are then computed given the distance to the star. These are compared to the contrast curve for the observation, which give the faintest detectable companion (at the 5σ level) to the star, in the observation band, as a function of angular separation from the star.

In cases where the same target star is observed in multiple epochs, and sometimes among different surveys (a common occurrence, the 22, 50, and 71 stars we use in this work would suggest a sample size of 143 target stars, but there are only 118 unique target stars between these three surveys with reliable age estimates), the additional elapsed time is taken into account. Simulated planets are generated at the earliest epoch as usual, and compared to that contrast curve. Their parameters are then used again, with orbital phase advanced forward by the time between observations (often a small effect for the planets to which these surveys are sensitive, a 30 AU orbit around a solar-type star has a 160 year period, and the typical time span between observations is at most about 3 years), the fluxes of the simulated planets are now computed in the new observation band, and compared to the new contrast curve. The process is repeated for as many observations as were conducted of the target star, and a simulated planet that is detectable in any of the observational epochs is considered detectable. Again, Nielsen et al. (2008) provides more details on these simulations, in particular their Fig. 3, 4, and 7.

3.1. Theoretical Models of Giant Planet Fluxes

In order to use the measured contrast curves for each observed target stars to determine which simulated planets could be detected, it is necessary to have a conversion from planet mass and age to NIR flux. As in Nielsen et al. (2008), we use the theoretical models of Burrows et al. (2003) and Baraffe et al. (2003) for the calculation of exoplanet flux, using the mass of each simulated planet and the age of the host target star, using the filter band (H or Ks) appropriate for the particular observation. In the cases of the GDPS (Lafrenière et al. 2007) and SDI (Biller et al. 2007) surveys, where the observation band was a specialized filter instead of the standard H bandpass, a correction factor is applied (see Section 3.2 for details). Though these two "hot start" models provide basically similar predictions, we perform our calculations with both, as the two models can predict significantly different NIR fluxes for exoplanets, depending on planet mass and stellar age, as shown in Fig. 2.

Since the publication of Nielsen et al. (2008), an additional set of theoretical models have been published by Fortney et al. (2008) for extrasolar planets for a range of masses and ages. The major difference between these new models and those from Burrows et al. (2003) and Baraffe et al. (2003) is that the Fortney et al. (2008) models are based heavily on the "core accretion" theory of planet formation (e.g. Hubickyj et al. (2005)), where giant planets are formed from an initial $\sim$10 $M_{\oplus}$ core accreting gas from the protoplanetary disk. After the brief luminous accretion phase, these models predict consistently fainter NIR fluxes than the "hot start" models (until $\sim$100 Myr to $\sim$1 Gyr, when the models overlap nicely, see Fig. 1 of Fortney et al. (2008)), which do not base their initial conditions on planetary core accretion models. For more detail, consult Figure 8, and Tables 1 and 2, of Fortney et al. (2008).

As is the case with the Burrows et al. (2003) models, the Fortney et al. (2008) models

do not cover the full range of planet parameters we consider here (masses between 0.5 and 15 M_{Jup}, ages from 1 Myr to 10 Gyr), since Fortney et al. (2008) limit their calculations to planets with T_{eff} >400K, leaving the consideration of cooler planets to future work. As a result, we extrapolate the models to masses below 1 M_{Jup} and above 10 M_{Jup}, and at larger ages (the age a planet cools below 400 K depends on the mass of the planet, ∼30 Myr for a 1 M_{Jup} planet, and ∼1 Gyr for a 10 M_{Jup} planet). While not an ideal solution, as we are ignoring the complicated physical processes taking places in planets as we cross these boundaries in exchange for simple relationships between NIR fluxes and age and mass, we believe that overall this method provides a good overall picture of the fluxes of extrasolar planets as predicted by the Fortney et al. (2008) models. In Fig. 2, we plot the initial gridpoints of both the Baraffe et al. (2003) and Burrows et al. (2003) models, as well as our extrapolations to the full range of parameter space. A similar plot comparing the predicted fluxes for the Baraffe et al. (2003) and Fortney et al. (2008) models is shown in Fig. 3. Our effort to map additional areas of model parameter space is worthwhile since this work is the first to apply these new core accretion models to the field of high contrast imaging surveys.

3.2. Narrowband to Broadband Colors

When we considered stars observed with the SDI method in Nielsen et al. (2008), we used a constant conversion from the broadband H magnitude predicted by the models to the measured contrast in the narrowband "off-methane" filter (SDI F1, 2% bandpass, centered at 1.575 μm (Close et al. 2005)). While this conversion factor was consistent with observed T6 objects (Biller et al. 2007), it would be expected to vary across a broad range of planet temperatures, corresponding to the large differences in ages and masses of the simulated planets. In this work, we used template spectra from the SpeX instrument of 132 low-mass objects, spanning spectral types from L0 to T8, to compute the difference

between broadband H and narrowband filters as a function of effective temperature (M. Liu, private communication). Spectral types are converted to effective temperature by the polynomial fit of Golimowski et al. (2004), their Table 4. SpeX spectra were obtained from the online SpeX Prism Spectral Libraries (e.g. Cruz et al. (2004), Kirkpatrick et al. (2006), and Burgasser (2007)). Since the reliability of the models at reproducing the methane band when modeling planet atmospheres is still uncertain, we prefer this method to purely using the synthetic spectra from the models to make this color correction.

For GDPS target stars, we use this conversion for the NIRI CH4-short filter, to convert the model's prediction of planetary H-band flux to this 6.5% bandpass filter, centered at 1.58 μm. For SDI target stars, we follow the steps of the data reduction used in computing contrast curves, computing planet fluxes for both the bluest "off-methane filter" (F1), and the "on methane filter" (F3) both with a 2% bandpass, centered at 1.575 and 1.625 μm, respectively. Just as is done for the survey images, the on-methane flux is subtracted from the off-methane flux, providing (for each value of effective temperature) the expected final flux in the subtracted image, as represented by the contrasts curves of Biller et al. (2007). For both the SDI and GDPS target stars, we use the appropriate effective temperatures predicted by the models to match these color corrections to simulated planets of each combination of age and mass.

To partially account for this effect in Nielsen et al. (2008), for SDI target stars, we had imposed an upper cut-off on planet mass, set by where the models predicted planet effective temperatures would rise above 1400 K for a given age. Above this temperature, the methane break would be so weak that subtracting the "on-methane" image from the "off-methane" image would simply remove all flux from the planet, as it is meant to do for the star. As a result, planets more massive than this limit were simply considered undetectable. With our more robust method that appropriately attenuates planet flux as a

function of temperature, it is no longer necessary for us to impose this rather crude binary cut for SDI targets.

In principle, an SDI observation of a non-methanated companion should not suffer from self-subtraction of the companion signal, as images in the three SDI filters are shifted by wavelength before subtraction. This step aligns the speckles in the images (which scale as $\frac{\lambda}{D}$, where λ is the observation wavelength and D is the diameter of the telescope), but misaligns any physical objects (where separation from the primary star on the detector is not a function of wavelength). As such, following subtraction of images from two different filters, a real companion should appear as a "dipole:" a positive and negative PSF, forming a radial line toward the primary star. The separation between the positive and negative parts of the dipole in the subtracted image would be given by $\Delta d \sim \frac{\Delta\lambda}{\lambda} d$, where Δd is the length of the dipole on the detector, $\Delta\lambda$ is the difference in wavelength between the two filters, and d is the separation on the detector between the primary star and the companion. The most extreme shift in filters for SDI observations is between the 1.575 μm and 1.625 μm filters, or 3%. Since the field of view for the NACO VLT SDI observations was only 2.5", the largest shift between positive and negative companions in the subtracted image would be 6.5 pixels. As the FWHM for these observations was typically 3.5 pixels, this dipole effect would easily be lost against the speckle background at large separations, and almost undetectable at small separations, where positive and negative companions would more closely overlap (Biller et al. 2007).

3.3. Completeness Plots

Using a similar method to Nielsen et al. (2008), we run Monte Carlo simulations of extrasolar planets at a grid of mass and semi-major axis points for each target star. For each star, then, we have what fraction of simulated planets could be detected as a function

of planet mass and semi-major axis. In order to combine these results over all 118 target stars, we again make use of the concept of the "planet fraction," or fraction of stars with a particular type of planet, defined such that

$$N(a, M) = \sum_{i=1}^{N_{obs}=118} f_p(a, M) P_i(a, M) \quad (1)$$

where N(a,M) is the number of planets we would expect to detect, as a function of semi-major axis and planet mass, N_{obs} is the number of stars observed, and $P_i(a, M)$ is the fraction of simulated planets, at a given combination of planet mass and semi-major axis, we could detected around the ith star in the sample. $f_p(a, M)$, then, is the fraction of stars that have a planet with a mass M and semi-major axis a. If every star had one Jupiter-mass planet at 5 AU, for example, then $f_p(5AU, 1M_{Jup}) = 1$, and the number of these Jupiter analogs we would expect to detect from the three surveys would simply be the sum of the detection efficiency for these planets around all target stars. That is, if we had 10 stars in our sample ($N_{obs} = 10$), and we had a 50% chance of detecting a Jupiter-like planet around each star ($P_i(5AU, 1M_{Jup}) = 0.5$), our expected number of detections of these planets would be 5.

In the case of not finding planets, as was the case for the three surveys of FGKM stars considered here, we can use the null result to set an upper limit on the planet fraction, f_p. If we assume that planet fraction is constant across all stars in our survey (we will reexamine this assumption in Section 3.5), we can remove f_p from the sum of Equation 1. Then, utilizing the Poisson distribution, where the probability of 0 detections given an expectation value of 3 (that is, $N(a, M) = 3$), is 5%, we can set the 95% confidence level upper limit on planet fraction with the equation

$$f_p(a, M) \leq \frac{3}{\sum_{i=1}^{N_{obs}} P_i(a, M)} \quad (2)$$

So, with the above example, where the expectation value is 5 for Jupiter-analogs over 10 target stars ($\sum_{i=1}^{N_{obs}=10} P_i(5AU, 1M_{Jup}) = 5$), not detecting any such planets would allow us to place a 95% confidence level upper limit of 60% on the fraction of stars with a Jupiter-twin ($f_p(a, M) < \frac{3}{5}$). Doing this over the entire grid of planet mass and semi-major axis allows us to plot what constraints can be placed on combinations of these planet parameters.

Fig. 4 gives the upper limit on planet fraction as a function of planet mass and orbital semi-major axis, using the models of Baraffe et al. (2003), with a similar plot using the theoretical models of Burrows et al. (2003) given in Fig. 5. We can place our strongest constraints on planets more massive than ∼4 M_{Jup} between 20 and 300 AU (fewer than 5% of stars can have such planets at 68% confidence); when stars of all spectral types are considered, the lower limit probed by direct imaging and the upper limit of the radial velocity method are still a factor of 5 apart. When we repeat the calculations using the models of Fortney et al. (2008), the decreased NIR flux predicted for giant planets reduces constraints that can be placed on extrasolar planets, with the "sweet spot" moving out to ∼80 AU, as seen in Fig. 6.

While we continue to run calculations using all three sets of models, and report the results here, for the sake of brevity we will henceforth only plot figures corresponding to the Baraffe et al. (2003) COND models. However, the figures appropriate to the Burrows et al. (2003) "hot-start" and Fortney et al. (2008) core accretion models are available in our supplement, available at this URL: http://exoplanet.as.arizona.edu/∼lclose/exoplanet2.html The supplement also contains individual completeness plots for each of our 118 target stars, using each of the three models of planet fluxes. Additionally, we summarize basic results

for all of our calculations in Table 3.

3.4. Testing Power Law Distributions for Extrasolar Planet Mass and Semi-Major Axis

These null results for extrasolar planets are also useful in setting constraints on the parameters of models for planet populations that assume power law distributions for the semi-major axis and mass distributions. Cumming et al. (2008) carefully examined the sensitivity of the Keck Planet Search, and determined that, over the range to which the radial velocity technique is sensitive (0.3 to 10 M_{Jup}, 2-2000 day orbital periods), planets follow a double power-law distribution with index -1.31 in mass and -0.61 in semi-major axis (-0.74 in orbital period). That is, $\frac{dN}{dM} \propto M^{-1.31}$ and $\frac{dN}{da} \propto a^{-0.61}$ (note that we define power law indices with respect to linear bins, $\frac{dN}{da}$, not the logarithmic bins of Cumming et al. (2008). Also, while Cumming et al. (2008) use α and β to refer to the power law indices for mass and period, respectively, we use α to refer to the power law index for semi-major axis).

Binarity is likely to disrupt planet formation, or at the very least change the underlying distribution of planets between binary planet hosts and single stars. Bonavita & Desidera (2007) have shown that the distribution of radial velocity planets for binary and single-star hosts are quite similar, and Holman & Wiegert (1999) suggest that planets are stable in binary systems with a planet semi-major axis $\gtrsim$20% of the binary separation. We take this into account for our consideration of power-law distributions of semi-major axis by excluding target stars with binaries within a factor of 5 of the planetary semi-major axis being considered. In Table 4, we give the results of a literature search for binaries among our target stars, including binary separation and binary type.

By adopting these power laws, and using the normalization of Fischer & Valenti (2005)

to give the total fraction of stars with planets, we can then predict how many planets these three surveys should have detected for various power law fits. If a large number of planets is predicted, our null result can be used to strongly exclude that model. If we accept the power-law distribution for mass of Cumming et al. (2008) and the normalization of Fischer & Valenti (2005), the two remaining parameters are the semi-major axis power-law index α, and the semi-major axis upper cut-off (that is, what maximum semi-major axis the distribution continues to until planets are no longer present). We illustrate this in Fig. 7, where we depict various models of the semi-major axis distribution, and the confidence with which we can reject them, using the models of Baraffe et al. (2003). For 12 different combinations of semi-major axis power law index and upper cut-off we give the percentage we can reject each of these 12 models in this figure. For the model of Cumming et al. (2008), with $\frac{dN}{da} \propto a^{-0.61}$, and at 95% confidence, the upper cut-off must be less than 65 AU, and less than 30 AU with 68% confidence.

We again use the theoretical models for planet fluxes of Baraffe et al. (2003), and consider a broader range of power-law index α and upper cut-off in Fig. 8. As before, the results from the two hot start models (Burrows et al. 2003; Baraffe et al. 2003) are generally similar, as the upper cut-offs must be less than 28 and 56 AU (68% and 95% confidence) for the Burrows et al. (2003) models. The fainter predicted fluxes from the Fortney et al. (2008) models reducing the areas of parameter space that our null result can exclude: the 68% and 95% confidence level upper limits for upper cut-off become 83 and 182 AU, for a -0.61 power law index.

3.5. The Dependence on Stellar Mass of the Frequency of Extrasolar Giant Planets

In Sections 3.3 and 3.4, we assume the distribution and frequency of giant planets is constant across all the stars in our survey. Johnson et al. (2007) show this assumption to be incorrect by examining the frequency of giant planets around stars in three mass bins from radial velocity surveys, and showing that more massive stars are more likely to harbor giant planets (see their Fig. 6). As in Nielsen et al. (2008), we divide the target stars into two samples, one containing only M stars, and the other with FGK stars (Our sample contains a single A star, HD 172555 A, with spectral type A5, with all our stars F2 or earlier. We include this A star with the FGK stars; however, observations of this single star are not sufficient to make any meaningful statements about the population of planets around A stars). We then imagine a planet fraction (f_p) with one value for M stars, and another for stars of earlier spectral types.

In Fig. 10 we use the Baraffe et al. (2003) models to show the upper limit that can be placed on the planet fraction for M stars. Since only 18 of the 118 target stars are M stars, the smaller sample size greatly reduces the constraints that can be placed on planet fraction near the center of the contours, and the outer edge in semi-major axis. Interestingly, the small separation edge of the contours is virtually unchanged between Figs. 4 and 10, indicating that the power with which these surveys can speak to the populations of short-period giant planets is entirely due to the M stars in the surveys.

Fig. 11 uses the models of Baraffe et al. (2003) to give the upper limit on planet fraction for the FGK stars in the survey. The result for long-period planets and within the central contours is much the same as for stars of all spectral types (Fig. 4), but the contours at the smallest values of semi-major axis march outward without the M stars to provide high contrasts at small angular separations.

A more satisfying way to address the issue of stellar mass dependence is to weight the results by target star mass, so that all stars in the survey can be applied to the result simultaneously. To do this, we construct a linear fit to the metallicity-corrected histogram from Fig. 6 of Johnson et al. (2007), to give a correction to planet fraction as a function of stellar mass, as we show in Fig. 9. (Here we assume that the relation found by Johnson et al. (2007) for short-period planets (less than six years) applies to the entire range of semi-major axis. While this assumption is obviously untested, in the absence of better data we believe it is a good starting point.) In the case of setting upper limits on planet fraction, we now allow planet fraction to become a function of stellar mass (M_*) in addition to planet mass and semi-major axis (M_p and a). In that case we can specify planet fraction for the stellar mass of a solar mass ($f_{p,1.0}(a, M_p)$), and find the upper limit as with Equation 2, but now including an extra term for the mass correction:

$$f_{p,1.0}(a, M_p) \leq \frac{3}{\sum_{i=1}^{N_{obs}} P_i(a, M_p) mc_{1.0}(M_{*,i})} \tag{3}$$

where $mc_{1.0}(M_{*,i})$ is the mass correction as a function of the stellar mass of the ith star in the sum, normalized to 1.0 $M_\odot$, and defined by $mc_{1.0}(M_*) = \frac{F_p(M_*)}{F_p(1.0M_\odot)}$, where F_p is the fraction of stars with a detected radial velocity planet as a function of stellar mass, using the linear fit to the Johnson et al. (2007) results. Again, going back to our earlier example, imagine that we have 10 stars, each with 50% completeness to Jupiter-like planets. If all 10 stars are 1 solar mass, then $mc_{1.0}(M_*) = \frac{F_p(1.0M_\odot)}{F_p(1.0M_\odot)} = 1$, and as before the upper limit on planet fraction (for the 95% confidence level, as given by the 3 in the numerator) is 60%. On the other hand, if only four of the ten target stars had masses of 1 $M_\odot$, and the remaining six had masses of 2.5 $M_\odot$, we must weight the results to account for the greater likelihood of stars of earlier spectral types to have planets. A 2.5 $M_\odot$ star is twice as likely to have a planet as a solar mass star (see Fig. 9), so for the four stars of 1 $M_\odot$, $mc_{1.0}(1.0M_\odot)$

remains 1, as before, while for the stars of 2.5 $M_\odot$, this factor doubles, $mc_{1.0}(2.5M_\odot) = 2$. In this case, Equation 2 becomes $f_{p,1.0}(a, M_p) \leq \frac{3}{0.5+0.5+0.5+0.5+1+1+1+1+1+1} = 3/8$ =37.5%. Including A stars in this fictional example almost doubles the constraint we can place on the fraction of stars with a giant planet. Similarly, M stars will be weighted against to account for their decreased likelihood of having planets. As an aside, we note that while our sample is spread across spectral type (1 A star, 8 F, 33 G, 58 K, and 18 M stars), only 18 of our target stars are more massive than the sun. Despite the increased probability of finding planets around higher mass target stars, these stars are intrinsically brighter, and so moving earlier in spectral type very quickly results in any potential planet photons being swamped by the glare of its host star (though the recent discoveries of planets around A stars, e.g. Marois et al. (2008), show that this difficulty can be overcome and produce exciting results).

In Fig. 12, we plot the upper limit on planet fraction for stars of 1 $M_\odot$, using Equation 3. When comparing Figs. 10 and 11 with Fig. 4, we see that the contours at small values of semi-major axis are set mainly by the 18 M stars in our sample, while the behavior at large separations and the depth of the contours at intermediate values of semi-major axis are set by the 100 FGK stars in the sample. So it is then not too surprising that Fig. 12 is quite similar to Fig. 4, with the contours corresponding to the smallest upper limits on planet fraction shrinking slightly, and the contour at lower semi-major axis moving to the right in the figure, as M stars are now given less weight.

Alternatively, instead of normalizing to solar-type stars, we can instead consider what constraints are placed on stars of 0.5 $M_\odot$ (about an M0 spectral type). The constraints should become more powerful, as we assume a global decrease in the planet fraction for massive planets around lower-mass stars. (Again, this applies strictly to massive planets, $>0.5M_{Jup}$. The direct imaging surveys considered here are not sensitive to Neptune mass

planets, which may be more common around M-stars: Endl et al. (2008) suggest that Hot Neptunes may be ∼4 times more prevalent orbiting M-stars than Hot Jupiters around FGK stars) In fact, the only result of this change is to multiply a constant factor by the right-hand-side of Equation 3 corresponding to the ratio of the likelihood of finding a planet around a solar mass star to that of finding a planet around a star of 0.5 $M_{\odot}$, or 1.5 in this case. We plot these limits on planet fraction for half solar mass stars in Fig. 13, with the models of Baraffe et al. (2003). As expected, the contours move outward, setting strong constraints on the frequency of giant planets in long-period orbits around M stars.

We also reconsider the implications of stellar mass on the constraints put on the power-law model for the semi-major axis distribution of extrasolar planets, as discussed in Section 3.4. Again, by using the linear fit to the results of Johnson et al. (2007), we boost the predicted number of planets for higher mass target stars, and suppress that number for lower mass stars. In Fig. 14 we show the same combination of three power law indices and four values of the upper cut-off as before, and the models of Baraffe et al. (2003), but now with the additional correction for the dependence of planet frequency on the stellar mass of each target star. The confidence level at which we can exclude each model drops compared to Fig. 7, as M stars are effectively given less weight. While the upper limit on planet fraction as a function of planet mass and semi-major axis is specific to a given stellar mass, Fig. 14 (and the next one, Fig. 15) need not be normalized to a specific spectral type. The Johnson et al. (2007) mass correction and the Fischer & Valenti (2005) planet fraction sets the absolute likelihood a given target star has a giant planet, which is used to calculate the predicted number of planets detected from our entire survey. Given our null result, this expectation value is used to set a confidence level with which the entire model (giant planet self-luminosity, giant planet fraction, dependence of planet fraction on stellar mass, and planet mass, semi-major axis, and orbital eccentricity distributions) can be rejected.

For the full range of power law index and upper cut-off, again with the Baraffe et al. (2003) models, we plot contours for the confidence level of rejection in Fig. 15. This figure is again generally similar to Fig. 8, but with the constraints slightly looser as M stars in the sample receive less weight. With the Johnson et al. (2007) mass correction, the 68% and 95% confidence level upper limits on the semi-major axis distribution cut-off are 37 and 82 AU for the Baraffe et al. (2003) models, respectively (without the mass correction, these were 30 and 65 AU). For the Fortney et al. (2008) models these move from 83 and 182 AU to 104 and 234 AU.

3.6. Ida & Lin (2004) Core Accretion Formation Models

As in Nielsen et al. (2008), we turn to the giant planet formation and dynamical evolution models of Ida & Lin (2004), which predict the final state of giant planets, mass and semi-major axis, following the core accretion scenario. We extract 200-300 planets from their Fig. 12, and use these masses and semi-major axes in our Monte Carlo simulations. We plot the predicted number of planets detected from these models in Fig. 16, with target stars divided by binarity. Even with our 118 target stars, without removing close binaries, not accounting for stellar mass (the Ida & Lin (2004) models were run with a 1 $M_{\odot}$ primary star), and using the planet luminosities of the Baraffe et al. (2003) models, the Monte Carlo simulations show that for each of the three cases of Ida & Lin (2004), we would expect to detect about 1 planet for each. In Nielsen et al. (2008), we could only exclude the cases of Ida & Lin (2004) A, B, and C at 45%, 49%, and 50% confidence, respectively, with the expanded target star sample here these rejection levels only become 45%, 59%, and 63% (using the Burrows et al. (2003) models to be consistent with Nielsen et al. (2008)). When using the models of Baraffe et al. (2003), the limits for the sample of this paper are 38%, 58%, and 62%. The models of Ida & Lin (2004) predict very few giant planets

in long-period orbits: fewer than 20% of the giant planets predicted by these models are beyond 10 AU, while our 68% confidence limit on the upper limit of the Cumming et al. (2008) power-law, 23 AU, gives 30% of giant planets in orbits beyond 10 AU. However, our current limits can neither confirm nor rule out the Ida & Lin (2004) populations.

4. Discussion

Overall, the conclusions from this work are largely similar to those of Nielsen et al. (2008), that extrasolar giant planets are rare at large separations around Sun-like or less massive stars. Even with the most pessimistic models for planet NIR fluxes (Fortney et al. 2008), and weighting against the M stars (which provide the most favorable contrasts for finding planets), we find that at 95% confidence, fewer than 20% of solar-mass stars can have a planet more massive than 4 M_{Jup} in an orbit between 123 and 218 AU. Also, a power-law model for the semi-major axis distribution of giant planets following the results of Cumming et al. (2008) must have a cut-off of 104 AU at 68% confidence, and 234 AU at 95% confidence, again using the Fortney et al. (2008) models and the Johnson et al. (2007) mass correction.

It is worth noting that there are additional models of giant planet distributions beyond what we consider here. Cumming et al. (2008) found a good fit to distributions of close-in giant planets from radial velocity work using a single power-law for the distribution of semi-major axis. It is also possible, however, that while this is a good fit for giant planets within $\sim$5 AU, it may not hold for planets at larger separations; perhaps a broken power law or some other distribution governs the population of giant planets in long period orbits. If all giant planets are formed beyond the snow line, perhaps the final distribution differs for planets that migrate inwards and those that remain beyond the snow line. Alternatively, there may be multiple methods of planet formation, such as the core accretion scenario

and the disk instability model (e.g. Ida & Lin (2004) vs. Boss (2007)), and the frequency with which each occurs is a function of distance from the star. Another possibility is that mass and semi-major axis are not independent distributions, which should become testable as the number of known exoplanets increases. Additionally, moving across spectral type may not only change the frequency of giant planets, but also their distributions of mass and semi-major axis. The analysis of Cumming et al. (2008) relied exclusively on solar-type (FGK) planet hosts, with the number of planets orbiting M stars being too small to draw any conclusions about a possible dependence of planet distributions on spectral type. These issues cannot be well addressed with further null results; they require a large number of detected planets at intermediate ($\sim$5-20 AU) and large ($>$20 AU) separations to make statistically significant statements on long-period giant planet populations.

Since this paper was first submitted, the discovery of several planet candidates, via direct imaging, was announced; planets were detected around the three stars, all of A spectral type, HR 8799 (Marois et al. 2008), Fomalhaut (Kalas et al. 2008), and β Pic (Lagrange et al. 2009). These exciting discoveries are consistent with the predictions of Johnson et al. (2007), as even though planets within 100 AU (like the three found around HR 8799) should be easier to detect around lower-mass stars (where the self-luminosity of the star is smaller), similar planets have not been found around stars of solar mass or smaller. However, each one of these planetary systems is different from the other. Moreover, all are around more massive stars than were analyzed here. Since the full survey papers for each of these discoveries have not yet been published, it is difficult to incorporate these results into our analysis of Sun-like (and less massive) stars.

5. Conclusions

We have used Monte Carlo simulations to examine the null result from three direct imaging surveys (Masciadri et al. 2005; Biller et al. 2007; Lafrenière et al. 2007) to set constraints on the population of extrasolar giant planets. We use three commonly cited sets of planet models (Burrows et al. 2003; Baraffe et al. 2003; Fortney et al. 2008) in order to reach conclusions as broad as possible. Doubling the sample size, as expected, increased the strength of our null results. However, including better modeling for giant planets–using the stellar mass dependence of giant planet frequency of Johnson et al. (2007), and the core-accretion based luminosity models of Fortney et al. (2008)–have actually loosened the constraints reported in Nielsen et al. (2008). There is still some uncertainty, however, in which if any of these models of planet luminosity is correct; likely the truth may fall in between that of the optimistic "hot start" models and the somewhat pessimistic "core accretion" model.

With the COND models of Baraffe et al. (2003), a planet more massive than 4 M_{Jup} is found around 20% or less of FGKM stars in orbits between 8.1 and 911 AU, at 68% confidence. These limits become 7.4 to 863 AU for Burrows et al. (2003), and 25 to 557 AU for the models of Fortney et al. (2008). At 95% confidence, 4 M_{Jup} (and larger) planets are found around fewer than 20% of stars between 22 and 507 AU, 21 and 479 AU, and 82 and 276 AU for the models of Baraffe et al. (2003), Burrows et al. (2003), and Fortney et al. (2008), respectively.

Using the power law distribution of Cumming et al. (2008), with index -0.61, the upper cut-off for the distribution of giant planets is found at 30 and 65 AU, at the 68% and 95% confidence levels, respectively, using the models of Baraffe et al. (2003). With the models of Burrows et al. (2003) these limits become 28 and 56 AU, and with the Fortney et al. (2008) models they are 83 and 182 AU.

When we apply the Johnson et al. (2007) dependency of planet fraction on stellar mass, the M stars in our sample (where we achieve the greatest sensitivity to planets), are weighted down to account for their decreased likelihood of hosting a giant planet. As a result, the improved null results cited above retreat to levels similar to those cited in Nielsen et al. (2008) and Lafrenière et al. (2007). Given our results, fewer than 20% of solar-type stars have a >4 M_{Jup} planet between 13 and 849 AU at 68% confidence with the Baraffe et al. (2003) models (also 13 and 805 AU for the models of Burrows et al. (2003), and 41 and 504 AU for the Fortney et al. (2008) models). At 95% confidence, for the models of Baraffe et al. (2003), Burrows et al. (2003), and Fortney et al. (2008), fewer than 20% of 1 $M_{\odot}$ stars have 4 M_{Jup} planets between 30 and 466 AU, 30 and 440 AU, and 123 and 218 AU, respectively.

Applying the Johnson et al. (2007) results to the Cumming et al. (2008) model for semi-major axis distribution, giant planets cannot exist beyond 37 and 82 AU for the Baraffe et al. (2003) models at 68% and 95% confidence. The 68% and 95% confidence figures become 36 and 82 AU for the Baraffe et al. (2003) models and 104 and 234 AU for the models of Fortney et al. (2008). In general, the Johnson et al. (2007) dependence of planet fraction on stellar mass makes direct imaging planet searches more difficult, as the stars most likely to harbor giant planets are also the most luminous, giving extreme contrast ratios between star and planet that impede planet detection.

We note that while the constraints on giant planet populations from this and other work have, for the first time, reached the equivalent of extrasolar "Kuiper Belts," there is still a gap ($\sim$5 - $\sim$30 AU) between these results for FGKM stars and those of radial velocity surveys, which focus more on the inner solar system. Delving into this unprobed region from the direct imaging side can be achieved two ways: increasing sensitivity to planets at small separations (achievable with dedicated planet finders using "extreme" adaptive optics, e.g.

GPI (Graham et al. 2007) and VLT-SPHERE (Boccaletti et al. 2008)), or with large-scale surveys to increase the sample size of target stars, such as the 500 hour Near-Infrared Coronagraphic Imager (NICI) survey at Gemini South (Chun et al. 2008). Our technique can be applied to the results from any direct imaging survey for giant exoplanets, requiring only the target list and achieved contrast curves. By building up the statistics of null results, it will be possible to more directly focus direct imaging efforts on where planets are most likely to exist, and create a fuller picture of the distribution of extrasolar giant planets. Additionally, such an analysis helps to put the survey into context with respect to previous work. There is also no limitation based on observation wavelength, even when target stars are observed by multiple surveys, since simulated planets are advanced in their orbits and compared to each contrast curve. As such, it will be interesting in future work to consider the results from L and M band surveys currently being conducted (e.g. Kasper et al. (2007)). Baraffe et al. (2003) and Burrows et al. (2003) predict planets with significantly lower contrasts to their parent stars at these longer wavelengths, and so the inclusion of results from such surveys could strengthen our null results, especially at large separations.

We are grateful to the anonymous referee for providing many helpful comments that improved the quality of this paper. We thank Beth Biller for the publication and compilation of the SDI contrast curves, as well as a large amount of useful input in preparing these simulations. We also thank Elena Masciadri for providing published contrast curves, and the authors of Lafrenière et al. (2007) for the careful preparation and publication of their achieved contrasts and observational techniques. We thank Eric Mamajek for a great deal of assistance in determining the ages of our target stars, as well as Michael Liu for providing the broadband-to-narrowband colors of low-mass objects. We thank Remi Soummer for the idea of presenting sensitivity to planets as a grid of

mass and semi-major axis points, and we thank Daniel Apai for presenting the idea of constructing a grid of semi-major axis power law indices and cut-offs. We also thank Rainer Lenzen, Thomas Henning, and Wolfgang Brandner for their important work in the original data gathering, and helpful comments over the course of the project. This work makes use of data from the European Southern Observatory, under Program 70.C - 0777D, 70.C - 0777E, 71.C-0029A, 74.C-0548, 74.C-0549, and 76.C-0094. Observations reported here were obtained at the MMT Observatory, a joint facility of the University of Arizona and the Smithsonian Institution. Based on observations obtained at the Gemini Observatory, which is operated by the Association of Universities for Research in Astronomy, Inc., under a cooperative agreement with the NSF on behalf of the Gemini partnership: the National Science Foundation (United States), the Science and Technology Facilities Council (United Kingdom), the National Research Council (Canada), CONICYT (Chile), the Australian Research Council (Australia), Ministério da Ciência e Tecnologia (Brazil) and SECYT (Argentina) This publication makes use of data products from the Two Micron All-Sky Survey, which is a joint project of the University of Massachusetts and the Infrared Processing and Analysis Center/California Institute of Technology, funded by the National Aeronautics and Space Administration and the National Science Foundation. This research has made use of the SIMBAD database, operated at CDS, Strasburg, France. ELN is supported by a Michelson Fellowship, without which this work would not have been possible. LMC was supported by an NSF CAREER award and by NASA's Origin of Solar Systems program.

REFERENCES

Abt, H. A. 1985, ApJS, 59, 95

Aitken, R. G. & Doolittle, E. 1932, New general catalogue of double stars within 120 of the North pole ... ([Washington, D.C.] Carnegie institution of Washington, 1932.)

Alcala, J. M., Krautter, J., Schmitt, J. H. M. M., Covino, E., Wichmann, R., & Mundt, R. 1995, A&AS, 114, 109

Ambruster, C. W., Brown, A., Fekel, F. C., Harper, G. M., Fabian, D., Wood, B., & Guinan, E. F. 1998, in Astronomical Society of the Pacific Conference Series, Vol. 154, Cool Stars, Stellar Systems, and the Sun, ed. R. A. Donahue & J. A. Bookbinder, 1205–+

Appenzeller, I., Thiering, I., Zickgraf, F.-J., Krautter, J., Voges, W., Chavarria, C., Kneer, R., Mujica, R., Pakull, M., Rosso, C., Ruzicka, F., Serrano, A., & Ziegler, B. 1998, ApJS, 117, 319

Arribas, S., Mediavilla, E., & Fuensalida, J. J. 1998, ApJ, 505, L43+

Baize, P. 1950, Journal des Observateurs, 33, 1

Baraffe, I., Chabrier, G., Barman, T. S., Allard, F., & Hauschildt, P. H. 2003, A&A, 402, 701

Bennett, N. W. W., Evans, D. S., & Laing, J. D. 1967, MNRAS, 137, 107

Bidelman, W. P. 1951, ApJ, 113, 304

—. 1985, ApJS, 59, 197

Biller, B. A., Close, L. M., Masciadri, E., Nielsen, E., Lenzen, R., Brandner, W., McCarthy, D., Hartung, M., Kellner, S., Mamajek, E., Henning, T., Miller, D., Kenworthy, M., & Kulesa, C. 2007, ApJS, 173, 143

Biller, B. A., Kasper, M., Close, L. M., Brandner, W., & Kellner, S. 2006, ApJ, 641, L141

Boccaletti, A., Carbillet, M., Fusco, T., Mouillet, D., Langlois, M., Moutou, C., & Dohlen, K. 2008, ArXiv e-prints, 807

Bonavita, M. & Desidera, S. 2007, A&A, 468, 721

Boss, A. P. 2007, ApJ, 661, L73

Bowyer, S., Lampton, M., Lewis, J., Wu, X., Jelinsky, P., & Malina, R. F. 1996, ApJS, 102, 129

Brandeker, A., Jayawardhana, R., Ivanov, V. D., & Kurtev, R. 2006, ApJ, 653, L61

Burgasser, A. J. 2007, ApJ, 659, 655

Burrows, A., Sudarsky, D., & Lunine, J. I. 2003, ApJ, 596, 587

Butler, R. P., Wright, J. T., Marcy, G. W., Fischer, D. A., Vogt, S. S., Tinney, C. G., Jones, H. R. A., Carter, B. D., Johnson, J. A., McCarthy, C., & Penny, A. J. 2006, ApJ, 646, 505

Chauvin, G., Lagrange, A.-M., Dumas, C., Zuckerman, B., Mouillet, D., Song, I., Beuzit, J.-L., & Lowrance, P. 2004, A&A, 425, L29

Chauvin, G., Lagrange, A.-M., Zuckerman, B., Dumas, C., Mouillet, D., Song, I., Beuzit, J.-L., Lowrance, P., & Bessell, M. S. 2005, A&A, 438, L29

Chen, Y. Q., Nissen, P. E., Benoni, T., & Zhao, G. 2001, A&A, 371, 943

Christian, D. J. & Mathioudakis, M. 2002, AJ, 123, 2796

Close, L. M., Lenzen, R., Guirado, J. C., Nielsen, E. L., Mamajek, E. E., Brandner, W., Hartung, M., Lidman, C., & Biller, B. 2005, Nature, 433, 286

Close, L. M. & Males, J. R. 2009, ArXiv e-prints

Close, L. M., Zuckerman, B., Song, I., Barman, T., Marois, C., Rice, E. L., Siegler, N., Macintosh, B., Becklin, E. E., Campbell, R., Lyke, J. E., Conrad, A., & Le Mignant, D. 2007, ApJ, 660, 1492

Cowley, A. P. 1976, PASP, 88, 95

Cowley, A. P., Hiltner, W. A., & Witt, A. N. 1967, AJ, 72, 1334

Cruz, K. L., Burgasser, A. J., Reid, I. N., & Liebert, J. 2004, ApJ, 604, L61

Cumming, A., Butler, R. P., Marcy, G. W., Vogt, S. S., Wright, J. T., & Fischer, D. A. 2008, PASP, 120, 531

Cutispoto, G., Pallavicini, R., Kuerster, M., & Rodono, M. 1995, A&A, 297, 764

Cutri, R. M., Skrutskie, M. F., van Dyk, S., Beichman, C. A., Carpenter, J. M., Chester, T., Cambresy, L., Evans, T., Fowler, J., Gizis, J., Howard, E., Huchra, J., Jarrett, T., Kopan, E. L., Kirkpatrick, J. D., Light, R. M., Marsh, K. A., McCallon, H., Schneider, S., Stiening, R., Sykes, M., Weinberg, M., Wheaton, W. A., Wheelock, S., & Zacarias, N. 2003, 2MASS All Sky Catalog of point sources. (The IRSA 2MASS All-Sky Point Source Catalog, NASA/IPAC Infrared Science Archive. http://irsa.ipac.caltech.edu/applications/Gator/)

Eggen, O. J. 1962, Royal Greenwich Observatory Bulletin, 51, 79

—. 1964, AJ, 69, 570

—. 1996, VizieR Online Data Catalog, 5008, 0

Eisenbeiss, T., Seifahrt, A., Mugrauer, M., Schmidt, T. O. B., Neuhäuser, R., & Roell, T. 2007, Astronomische Nachrichten, 328, 521

Endl, M., Cochran, W. D., Wittenmyer, R. A., & Boss, A. P. 2008, ApJ, 673, 1165

Evans, D. S. 1961, Royal Greenwich Observatory Bulletin, 48, 389

Fabricius, C. & Makarov, V. V. 2000, A&A, 356, 141

Fan, X., Strauss, M. A., Becker, R. H., White, R. L., Gunn, J. E., Knapp, G. R., Richards, G. T., Schneider, D. P., Brinkmann, J., & Fukugita, M. 2006, AJ, 132, 117

Favata, F., Barbera, M., Micela, G., & Sciortino, S. 1993, A&A, 277, 428

—. 1995, A&A, 295, 147

Favata, F., Micela, G., & Sciortino, S. 1997, A&A, 322, 131

Fernández, D., Figueras, F., & Torra, J. 2008, A&A, 480, 735

Fischer, D. A. & Valenti, J. 2005, ApJ, 622, 1102

Fleming, T. A., Gioia, I. M., & Maccacaro, T. 1989, ApJ, 340, 1011

Fortney, J. J., Marley, M. S., Saumon, D., & Lodders, K. 2008, ArXiv e-prints, 805

Gaidos, E. J., Henry, G. W., & Henry, S. M. 2000, AJ, 120, 1006

Gliese, W. & Jahreiß, H. 1979, A&AS, 38, 423

Gliese, W. & Jahreiss, H. 1991, NASA STI/Recon Technical Report A, 92, 33932

Golimowski, D. A., Leggett, S. K., Marley, M. S., Fan, X., Geballe, T. R., Knapp, G. R., Vrba, F. J., Henden, A. A., Luginbuhl, C. B., Guetter, H. H., Munn, J. A., Canzian, B., Zheng, W., Tsvetanov, Z. I., Chiu, K., Glazebrook, K., Hoversten, E. A., Schneider, D. P., & Brinkmann, J. 2004, AJ, 127, 3516

Gould, A. & Chanamé, J. 2004, ApJS, 150, 455

Graham, J. R., Macintosh, B., Doyon, R., Gavel, D., Larkin, J., Levine, M., Oppenheimer, B., Palmer, D., Saddlemyer, L., Sivaramakrishnan, A., Veran, J.-P., & Wallace, K. 2007, ArXiv e-prints, 704

Gray, R. O., Corbally, C. J., Garrison, R. F., McFadden, M. T., Bubar, E. J., McGahee, C. E., O'Donoghue, A. A., & Knox, E. R. 2006a, AJ, 132, 161

—. 2006b, AJ, 132, 161

Gray, R. O., Corbally, C. J., Garrison, R. F., McFadden, M. T., & Robinson, P. E. 2003a, AJ, 126, 2048

—. 2003b, AJ, 126, 2048

Hale, A. 1994, AJ, 107, 306

Harlan, E. A. 1974, AJ, 79, 682

Harlan, E. A. & Taylor, D. C. 1970a, AJ, 75, 507

—. 1970b, AJ, 75, 165

Heard, J. F. 1956, Publications of the David Dunlap Observatory, 2, 107

Helmer, L., Fabricius, C., Einicke, O. H., & Thoburn, C. 1983, A&AS, 53, 223

Henry, T. J., Soderblom, D. R., Donahue, R. A., & Baliunas, S. L. 1996, AJ, 111, 439

Herbig, G. H. & Spalding, Jr., J. F. 1955, ApJ, 121, 118

Holberg, J. B., Oswalt, T. D., & Sion, E. M. 2002, ApJ, 571, 512

Holden, F. 1977, PASP, 89, 582

Holman, M. J. & Wiegert, P. A. 1999, AJ, 117, 621

Hormuth, F., Brandner, W., Hippler, S., Janson, M., & Henning, T. 2007, A&A, 463, 707

Houk, N. 1978, Michigan catalogue of two-dimensional spectral types for the HD stars (Ann Arbor : Dept. of Astronomy, University of Michigan : distributed by University Microfilms International, 1978-)

Houk, N. 1982, in Michigan Spectral Survey, Ann Arbor, Dep. Astron., Univ. Michigan, 3, (1982)

Houk, N. & Cowley, A. P. 1975, Michigan Catalogue of two-dimensional spectral types for the HD star (Ann Arbor: University of Michigan, Departement of Astronomy, 1975)

Houk, N. & Smith-Moore, M. 1988, in Michigan Spectral Survey, Ann Arbor, Dept. of Astronomy, Univ. Michigan (Vol. 4), (1988)

Hubickyj, O., Bodenheimer, P., & Lissauer, J. J. 2005, Icarus, 179, 415

Ida, S. & Lin, D. N. C. 2004, ApJ, 604, 388

Israelian, G., Santos, N. C., Mayor, M., & Rebolo, R. 2004, A&A, 414, 601

Itoh, Y., Hayashi, M., Tamura, M., Tsuji, T., Oasa, Y., Fukagawa, M., Hayashi, S. S., Naoi, T., Ishii, M., Mayama, S., Morino, J.-i., Yamashita, T., Pyo, T.-S., Nishikawa, T., Usuda, T., Murakawa, K., Suto, H., Oya, S., Takato, N., Ando, H., Miyama, S. M., Kobayashi, N., & Kaifu, N. 2005, ApJ, 620, 984

Jayawardhana, R., Hartmann, L., Fazio, G., Fisher, R. S., Telesco, C. M., & Piña, R. K. 1999, ApJ, 521, L129

Johnson, J. A., Butler, R. P., Marcy, G. W., Fischer, D. A., Vogt, S. S., Wright, J. T., & Peek, K. M. G. 2007, ApJ, 670, 833

Jones, B. F., Fischer, D., Shetrone, M., & Soderblom, D. R. 1997, AJ, 114, 352

Jones, B. F., Fischer, D., & Soderblom, D. R. 1999, AJ, 117, 330

Kalas, P., Graham, J. R., Chiang, E., Fitzgerald, M. P., Clampin, M., Kite, E. S., Stapelfeldt, K., Marois, C., & Krist, J. 2008, Science, 322, 1345

Kasper, M., Apai, D., Janson, M., & Brandner, W. 2007, A&A, 472, 321

Kirkpatrick, J. D., Barman, T. S., Burgasser, A. J., McGovern, M. R., McLean, I. S., Tinney, C. G., & Lowrance, P. J. 2006, ApJ, 639, 1120

Lafrenière, D., Doyon, R., Marois, C., Nadeau, D., Oppenheimer, B. R., Roche, P. F., Rigaut, F., Graham, J. R., Jayawardhana, R., Johnstone, D., Kalas, P. G., Macintosh, B., & Racine, R. 2007, ApJ, 670, 1367

Lagrange, A.-M., Gratadour, D., Chauvin, G., Fusco, T., Ehrenreich, D., Mouillet, D., Rousset, G., Rouan, D., Allard, F., Gendron, É., Charton, J., Mugnier, L., Rabou, P., Montri, J., & Lacombe, F. 2009, A&A, 493, L21

Lambert, D. L. & Reddy, B. E. 2004, MNRAS, 349, 757

Leaton, B. R. & Pagel, B. E. J. 1960, MNRAS, 120, 317

Lenzen, R., Close, L., Brandner, W., Biller, B., & Hartung, M. 2004, in Ground-based Instrumentation for Astronomy. Edited by Alan F. M. Moorwood and Iye Masanori. Proceedings of the SPIE, Volume 5492, pp. 970-977 (2004)., ed. A. F. M. Moorwood & M. Iye, 970–977

Lépine, S. & Shara, M. M. 2005, AJ, 129, 1483

Lippincott, S. L. & MacDowall, R. J. 1979, PASP, 91, 471

Liu, M. C. 2004, Science, 305, 1442

López-Santiago, J., Montes, D., Crespo-Chacón, I., & Fernández-Figueroa, M. J. 2006, ApJ, 643, 1160

Lowrance, P. J., Becklin, E. E., Schneider, G., Kirkpatrick, J. D., Weinberger, A. J., Zuckerman, B., Dumas, C., Beuzit, J.-L., Plait, P., Malumuth, E., Heap, S., Terrile, R. J., & Hines, D. C. 2005, AJ, 130, 1845

Luhman, K. L., Allers, K. N., Jaffe, D. T., Cushing, M. C., Williams, K. A., Slesnick, C. L., & Vacca, W. D. 2007a, ApJ, 659, 1629

Luhman, K. L., Patten, B. M., Marengo, M., Schuster, M. T., Hora, J. L., Ellis, R. G., Stauffer, J. R., Sonnett, S. M. andWinston, E., Gutermuth, R. A., Megeath, S. T., & Fazio, G. G. 2007b, ApJ, 654, 570

Makarov, V. V., Zacharias, N., Hennessy, G. S., Harris, H. C., & Monet, A. K. B. 2007, ApJ, 668, L155

Malaroda, S. 1975, AJ, 80, 637

Mallik, S. V., Parthasarathy, M., & Pati, A. K. 2003, A&A, 409, 251

Mamajek, E. E. & Hillenbrand, L. A. 2008, ArXiv e-prints, 807

Marois, C., Lafrenière, D., Doyon, R., Macintosh, B., & Nadeau, D. 2006, ApJ, 641, 556

Marois, C., Macintosh, B., Barman, T., Zuckerman, B., Song, I., Patience, J., Lafrenière, D., & Doyon, R. 2008, Science, 322, 1348

Masciadri, E., Mundt, R., Henning, T., Alvarez, C., & Barrado y Navascués, D. 2005, ApJ, 625, 1004

Mathioudakis, M., Drake, J. J., Craig, N., Kilkenny, D., Doyle, J. G., Sirk, M. M., Dupuis, J., Fruscione, A., Christian, C. A., & Abbott, M. J. 1995, A&A, 302, 422

McCaughrean, M. J., Close, L. M., Scholz, R.-D., Lenzen, R., Biller, B., Brandner, W., Hartung, M., & Lodieu, N. 2004, A&A, 413, 1029

Metchev, S. A. & Hillenbrand, L. A. 2004, ApJ, 617, 1330

Montes, D., López-Santiago, J., Fernández-Figueroa, M. J., & Gálvez, M. C. 2001a, A&A, 379, 976

Montes, D., López-Santiago, J., Gálvez, M. C., Fernández-Figueroa, M. J., De Castro, E., & Cornide, M. 2001b, MNRAS, 328, 45

Mora, A., Merín, B., Solano, E., Montesinos, B., de Winter, D., Eiroa, C., Ferlet, R., Grady, C. A., Davies, J. K., Miranda, L. F., Oudmaijer, R. D., Palacios, J., Quirrenbach, A., Harris, A. W., Rauer, H., Cameron, A., Deeg, H. J., Garzón, F., Penny, A., Schneider, J., Tsapras, Y., & Wesselius, P. R. 2001, A&A, 378, 116

Morgan, W. W. & Keenan, P. C. 1973, ARA&A, 11, 29

Mugrauer, M., Neuhäuser, R., Guenther, E. W., Hatzes, A. P., Huélamo, N., Fernández, M., Ammler, M., Retzlaff, J., König, B., Charbonneau, D., Jayawardhana, R., & Brandner, W. 2004, A&A, 417, 1031

Nadal, R., Pedoussaut, A., Ginestet, N., & Carquillat, J.-M. 1974, A&A, 37, 191

Nesterov, V. V., Kuzmin, A. V., Ashimbaeva, N. T., Volchkov, A. A., Röser, S., & Bastian, U. 1995, A&AS, 110, 367

Neuhauser, R. & Brandner, W. 1998, A&A, 330, L29

Neuhäuser, R., Guenther, E., Mugrauer, M., Ott, T., & Eckart, A. 2002, A&A, 395, 877

Nielsen, E. L., Close, L. M., Biller, B. A., Masciadri, E., & Lenzen, R. 2008, ApJ, 674, 466

Nielsen, E. L., Close, L. M., Guirado, J. C., Biller, B. A., Lenzen, R., Brandner, W., Hartung, M., & Lidman, C. 2005, Astronomische Nachrichten, 326, 1033

Noyes, R. W., Weiss, N. O., & Vaughan, A. H. 1984, ApJ, 287, 769

Oswalt, T. D., Hintzen, P. M., & Luyten, W. J. 1988, ApJS, 66, 391

Pallavicini, R., Pasquini, L., & Randich, S. 1992, A&A, 261, 245

Pasquini, L., Liu, Q., & Pallavicini, R. 1994, A&A, 287, 191

Perry, C. L. 1969, AJ, 74, 705

Perryman, M. A. C., Lindegren, L., Kovalevsky, J., Hoeg, E., Bastian, U., Bernacca, P. L., Crézé, M., Donati, F., Grenon, M., van Leeuwen, F., van der Marel, H., Mignard, F., Murray, C. A., Le Poole, R. S., Schrijver, H., Turon, C., Arenou, F., Froeschlé, M., & Petersen, C. S. 1997, A&A, 323, L49

Potter, D., Martín, E. L., Cushing, M. C., Baudoz, P., Brandner, W., Guyon, O., & Neuhäuser, R. 2002, ApJ, 567, L133

Pounds, K. A., Allan, D. J., Barber, C., Barstow, M. A., Bertram, D., Branduardi-Raymont, G., Brebner, G. E. C., Buckley, D., Bromage, G. E., Cole, R. E., Courtier, M., Cruise, A. M., Culhane, J. L., Denby, M., Donoghue, D. O., Dunford, E., Georgantopoulos, I., Goodall, C. V., Gondhalekar, P. M., Gourlay, J. A., Harris, A. W., Hassall, B. J. M., Hellier, C., Hodgkin, S., Jeffries, R. D., Kellett, B. J., Kent, B. J., Lieu, R., Lloyd, C., McGale, P., Mason, K. O., Matthews, L., Mittaz, J. P. D., Page, C. G., Pankiewicz, G. S., Pike, C. D., Ponman, T. J., Puchnarewicz, E. M., Pye, J. P., Quenby, J. J., Ricketts, M. J., Rosen, S. R., Sansom, A. E., Sembay, S., Sidher, S., Sims, M. R., Stewart, B. C., Sumner, T. J., Vallance, R. J., Watson, M. G.,

Warwick, R. S., Wells, A. A., Willingale, R., Willmore, A. P., Willoughby, G. A., & Wonnacott, D. 1993, MNRAS, 260, 77

Poveda, A., Herrera, M. A., Allen, C., Cordero, G., & Lavalley, C. 1994, Revista Mexicana de Astronomia y Astrofisica, 28, 43

Pye, J. P., McGale, P. A., Allan, D. J., Barber, C. R., Bertram, D., Denby, M., Page, C. G., Ricketts, M. J., Stewart, B. C., & West, R. G. 1995, MNRAS, 274, 1165

Randich, S., Gratton, R., & Pallavicini, R. 1993, A&A, 273, 194

Randich, S., Pallavicini, R., Meola, G., Stauffer, J. R., & Balachandran, S. C. 2001, A&A, 372, 862

Reid, I. N., Hawley, S. L., & Gizis, J. E. 1995, AJ, 110, 1838

Roeser, S. & Bastian, U. 1988, A&AS, 74, 449

Rossiter, R. A. 1955, Publications of Michigan Observatory, 11, 1

Rufener, F. & Bartholdi, P. 1982, A&AS, 48, 503

Santos, N. C., Israelian, G., & Mayor, M. 2004, A&A, 415, 1153

Sato, K. & Kuji, S. 1990, A&AS, 85, 1069

Schild, R. E. 1973, AJ, 78, 37

Schwope, A., Hasinger, G., Lehmann, I., Schwarz, R., Brunner, H., Neizvestny, S., Ugryumov, A., Balega, Y., Trümper, J., & Voges, W. 2000, Astronomische Nachrichten, 321, 1

Simon, T. & Drake, S. A. 1993, AJ, 106, 1660

Soderblom, D. R., Jones, B. F., Balachandran, S., Stauffer, J. R., Duncan, D. K., Fedele, S. B., & Hudon, J. D. 1993a, AJ, 106, 1059

Soderblom, D. R., King, J. R., & Henry, T. J. 1998, AJ, 116, 396

Soderblom, D. R., King, J. R., Siess, L., Jones, B. F., & Fischer, D. 1999, AJ, 118, 1301

Soderblom, D. R., Pilachowski, C. A., Fedele, S. B., & Jones, B. F. 1993b, AJ, 105, 2299

Song, I., Bessell, M. S., & Zuckerman, B. 2002, ApJ, 581, L43

Song, I., Zuckerman, B., & Bessell, M. S. 2003, ApJ, 599, 342

Sozzetti, A., Udry, S., Zucker, S., Torres, G., Beuzit, J. L., Latham, D. W., Mayor, M., Mazeh, T., Naef, D., Perrier, C., Queloz, D., & Sivan, J.-P. 2006, A&A, 449, 417

Stephenson, C. B. 1960, AJ, 65, 60

Stocke, J. T., Morris, S. L., Gioia, I. M., Maccacaro, T., Schild, R., Wolter, A., Fleming, T. A., & Henry, J. P. 1991, ApJS, 76, 813

Strassmeier, K., Washuettl, A., Granzer, T., Scheck, M., & Weber, M. 2000, A&AS, 142, 275

Swain, M. R., Vasisht, G., & Tinetti, G. 2008, Nature, 452, 329

Torres, C. A. O., da Silva, L., Quast, G. R., de la Reza, R., & Jilinski, E. 2000, AJ, 120, 1410

Upgren, A. R. & Staron, R. T. 1970, ApJS, 19, 367

Vyssotsky, A. N., Janssen, E. M., Miller, W. J., & Walther, M. E. 1946, ApJ, 104, 234

Waite, I. A., Carter, B. D., Marsden, S. C., & Mengel, M. W. 2005, Publications of the Astronomical Society of Australia, 22, 29

Webb, R. A., Zuckerman, B., Platais, I., Patience, J., White, R. J., Schwartz, M. J., & McCarthy, C. 1999, ApJ, 512, L63

Wichmann, R., Schmitt, J. H. M. M., & Hubrig, S. 2003, A&A, 399, 983

Wilson, Jr., R. H. 1954, AJ, 59, 132

Wright, J. T., Marcy, G. W., Butler, R. P., & Vogt, S. S. 2004, ApJS, 152, 261

Zboril, M., Byrne, P. B., & Rolleston, W. R. J. R. 1997, MNRAS, 284, 685

Zuckerman, B. & Song, I. 2004, ARA&A, 42, 685

Zuckerman, B., Song, I., & Bessell, M. S. 2004, ApJ, 613, L65

Zuckerman, B., Song, I., Bessell, M. S., & Webb, R. A. 2001a, ApJ, 562, L87

Zuckerman, B., Webb, R. A., Schwartz, M., & Becklin, E. E. 2001b, ApJ, 549, L233

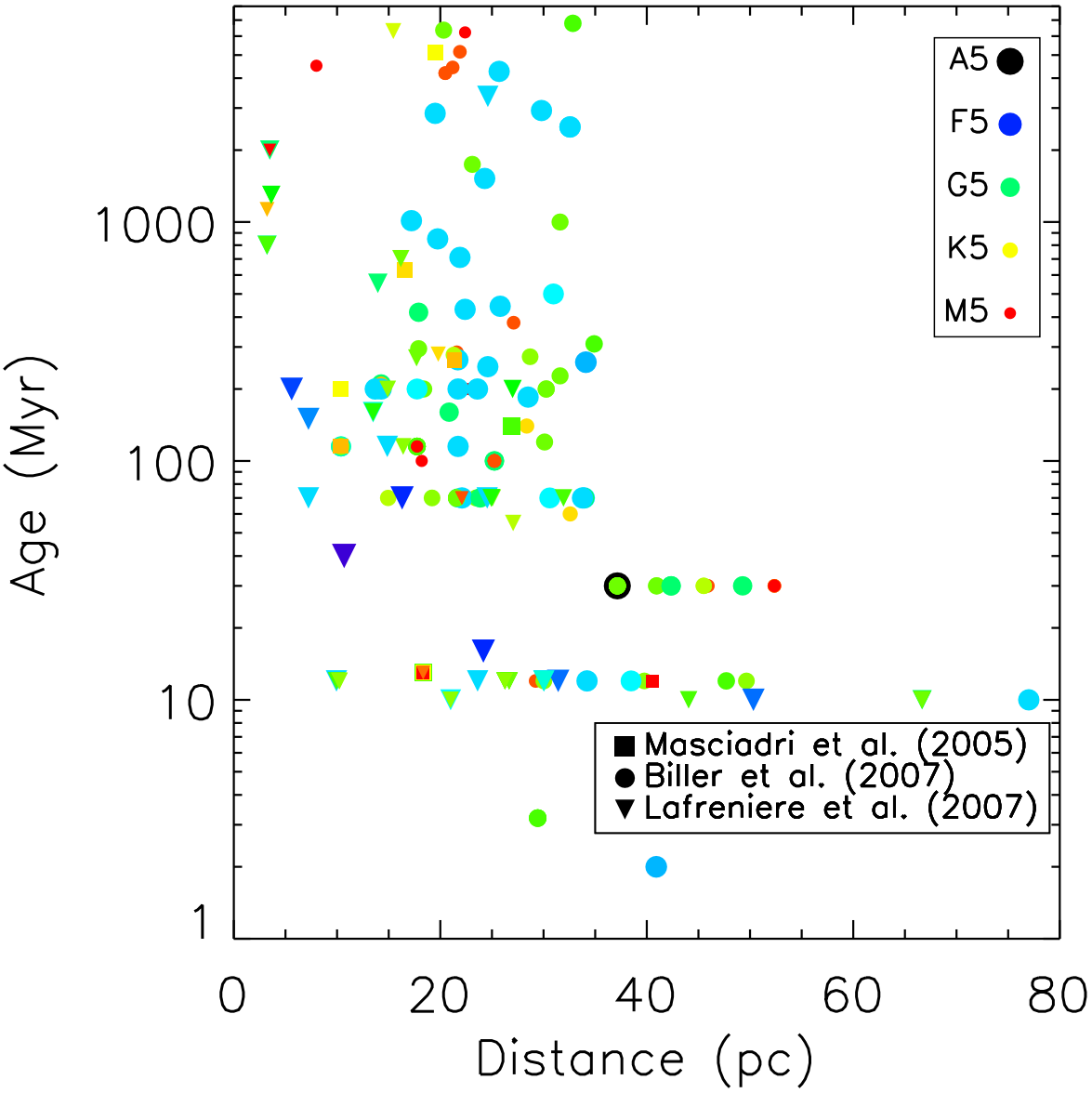

Fig. 1.— The 118 unique stars used in this paper, collected from the direct imaging planet surveys of Masciadri et al. (2005) (squares), Biller et al. (2007) (circles), and Lafrenière et al. (2007) (Triangles). Table 1 gives other properties of these stars, and Table 2 provides details on how the individual ages were determined. The median target star is a 160 Myr K1 star at 24 pc. The size and color of the plotting symbols corresponds to the spectral of each target star. The top legend gives the conversion between size and color of the plotting symbol and spectral type: the color scheme follows the visible spectrum, with early-type stars represented by large dark purple symbols, while late-type stars are small red symbols.

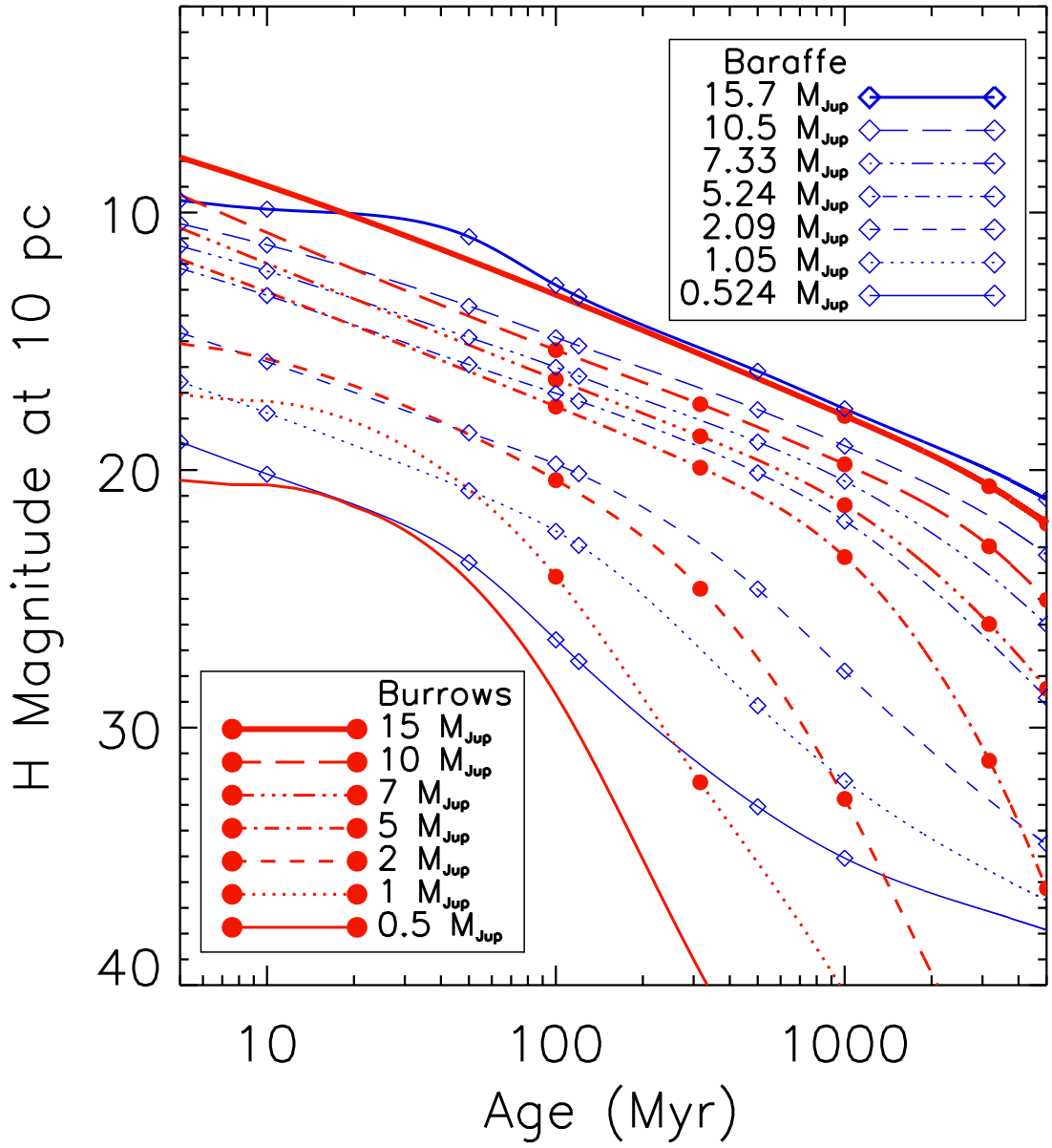

Fig. 2.— A plot of the age and H magnitude of planets, for different masses, as predicted by the Baraffe et al. (2003) and Burrows et al. (2003) models, represented by the thin blue lines and the thick red lines, respectively. The diamonds and circles are the H magnitudes given by the models themselves, while the lines show the interpolation and extrapolations beyond these points that we use when assigning H magnitudes to the simulated planets. The COND models of Baraffe et al. (2003) required very little extrapolation to fill the range of parameter space shown here, while far more extrapolation is required for the Burrows et al. (2003) models, especially at young ages and small masses.

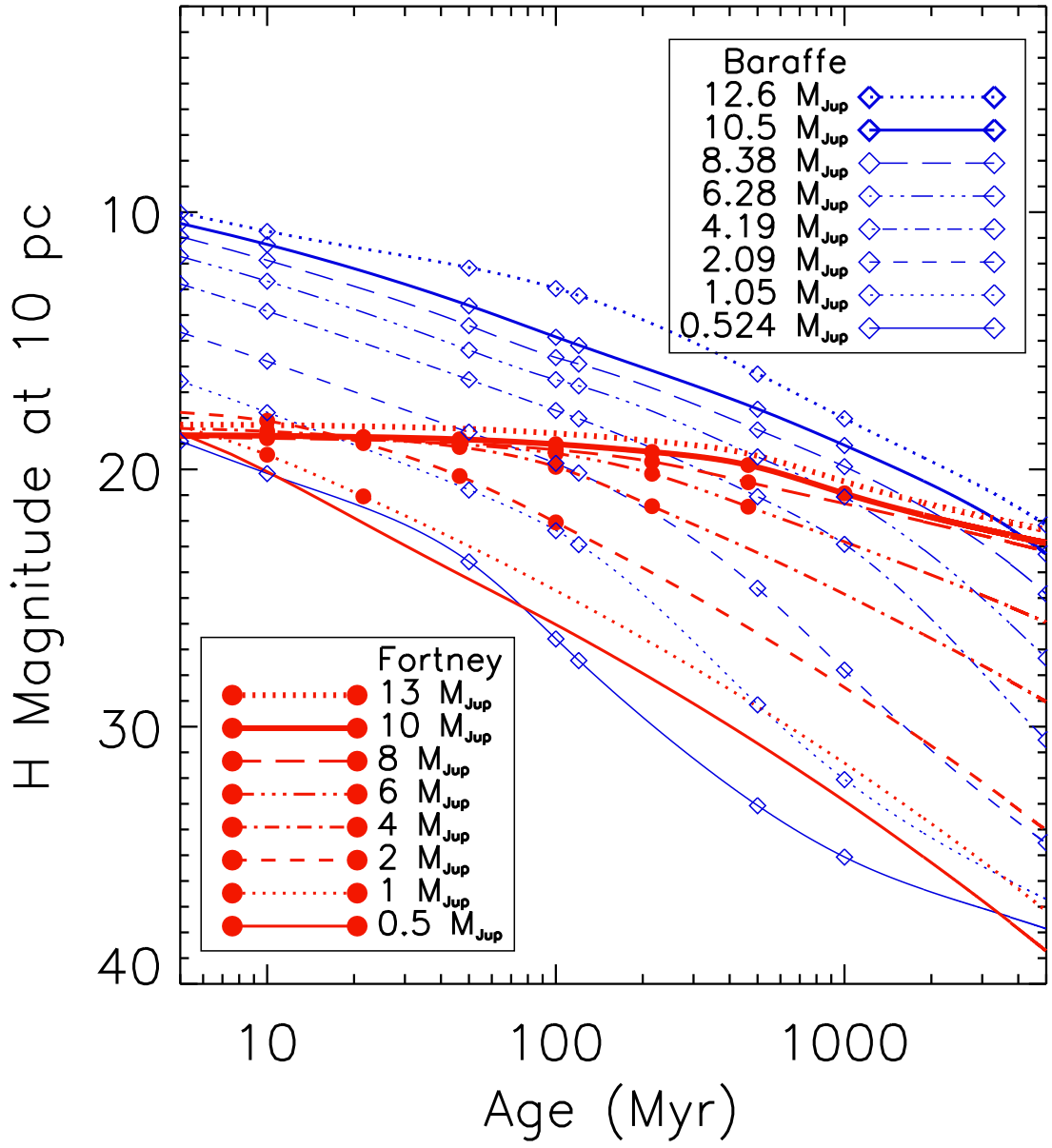

Fig. 3.— As with Fig. 2, a plot of the predicted fluxes of extrasolar planets of Baraffe et al. (2003), again represented by blue lines and open diamonds, this time plotted against the core accretion models of Fortney et al. (2008), the red lines with filled circles. In order to fill the parameter space of planet mass and stellar age we consider, it is necessary to extrapolate the Fortney et al. (2008) H magnitudes beyond the grid points of the models themselves, especially at larger ages and smaller masses.

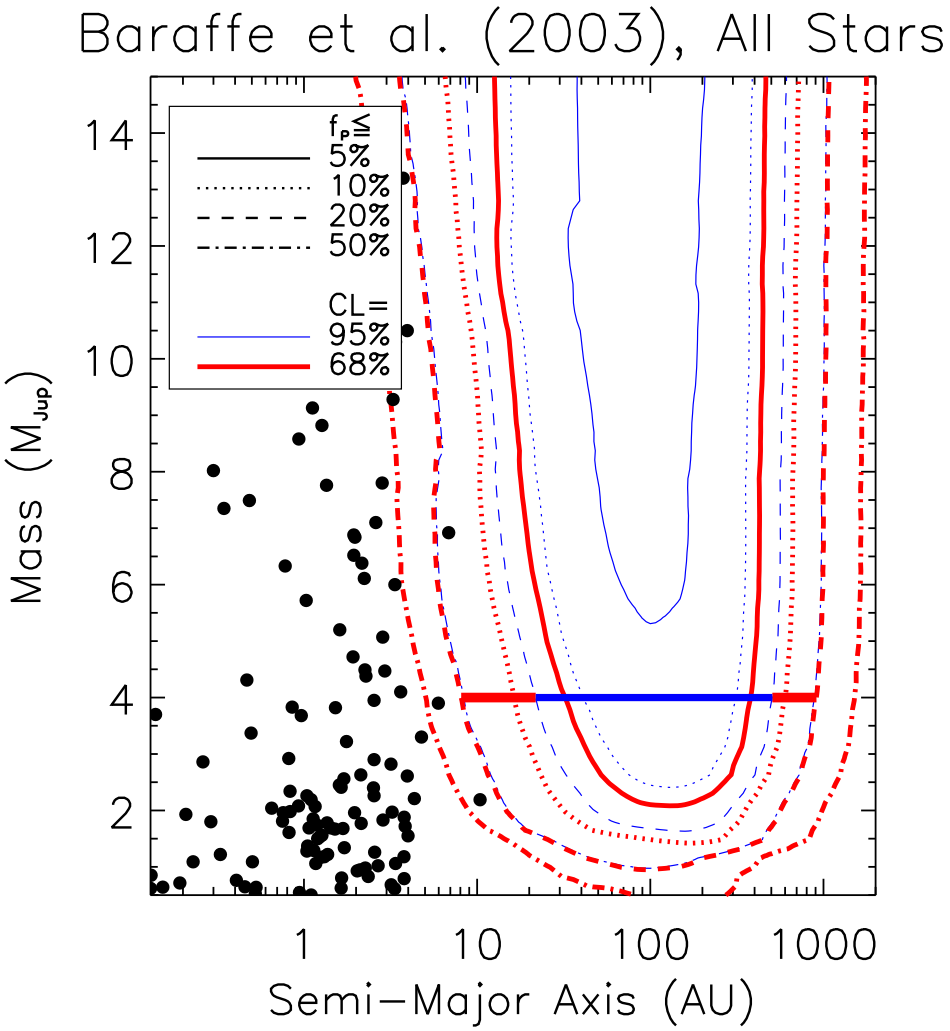

Fig. 4.— The upper limit on planet fraction (f_p, the fraction of stars with a planet of a given mass and semi-major axis, see Equation 1), at the 95% (blue, thin lines) and 68% (red, thick lines) confidence levels, using the theoretical models of Baraffe et al. (2003). With 95% confidence, we can say that less than 1 in 20 stars has a planet more massive than 8 M_{Jup} between 50 and 160 AU (constrained by the solid blue, thin curve). We plot a horizontal fiducial bar (again, with a thick red line and thin blue line) at 4 M_{Jup}, intersecting the f_p $\leq$20% contour at both 68% confidence (outer contour, thick red line) and 95% (inner contour, thin blue line). Hence, the horizontal line at the bottom right of the figure suggests no more than 1 in 5 stars would have a planet more massive than 4 M_{Jup} from 8.1 to 911 AU at the 68% confidence level, and between 22 and 507 AU at the 95% confidence level. Known radial velocity planets are shown as filled circles for comparison.

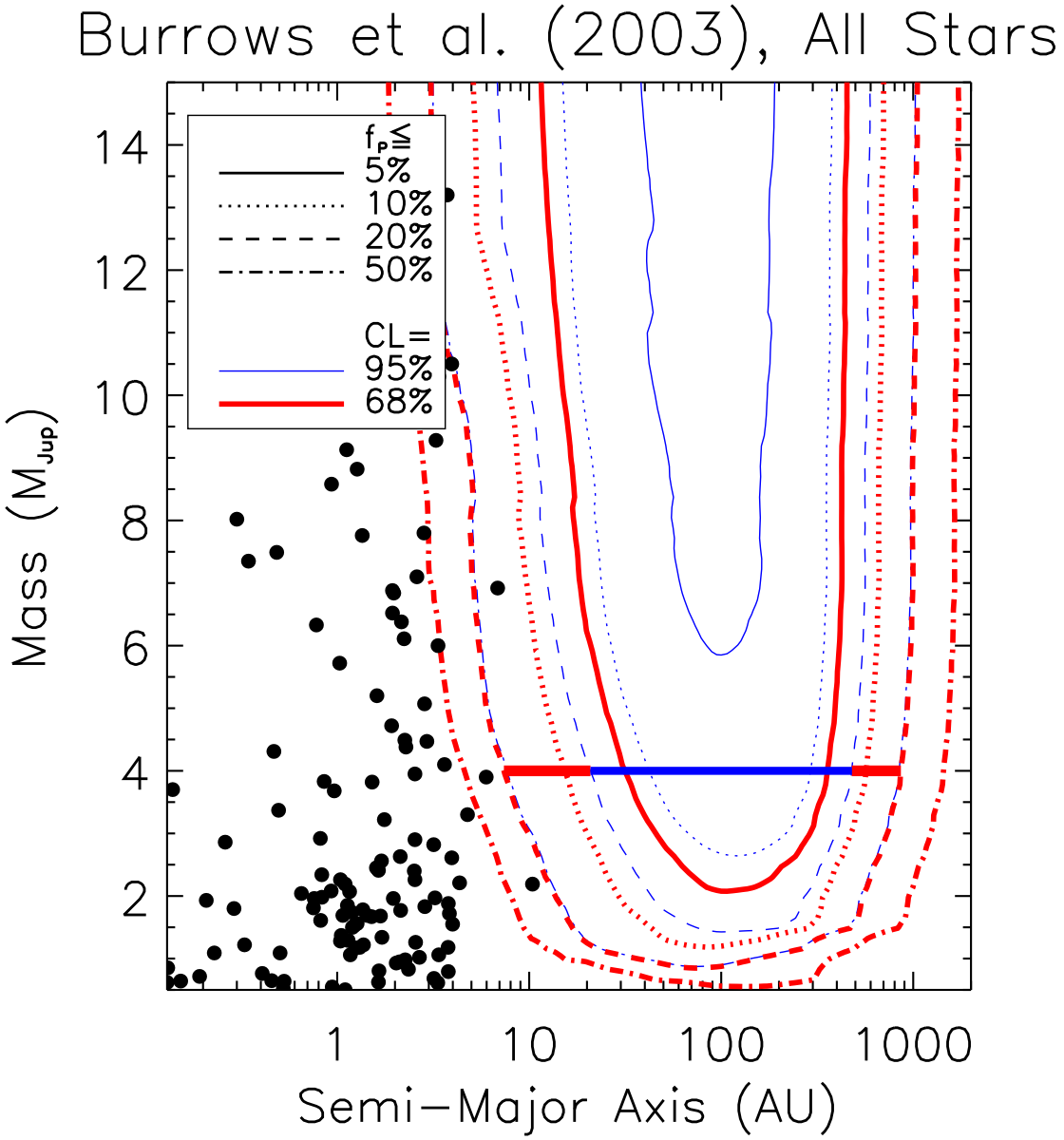

Fig. 5.— As with Fig. 4, the upper limit on planet fraction only now using the theoretical models of Burrows et al. (2003). The overall shape of the graph is quite similar, so with 95% confidence, we can place an upper limit on planet fraction of 5% for planets larger than 8 M_{Jup} with semi-major axis between 55 and 130 AU. As before, radial velocity planets are plotted as solid circles. The fiducial $f_p \leq$20% limits for 4 M_{Jup} are between 7.4 and 863 AU at 68% confidence, and 21 to 479 for the 95% confidence level.

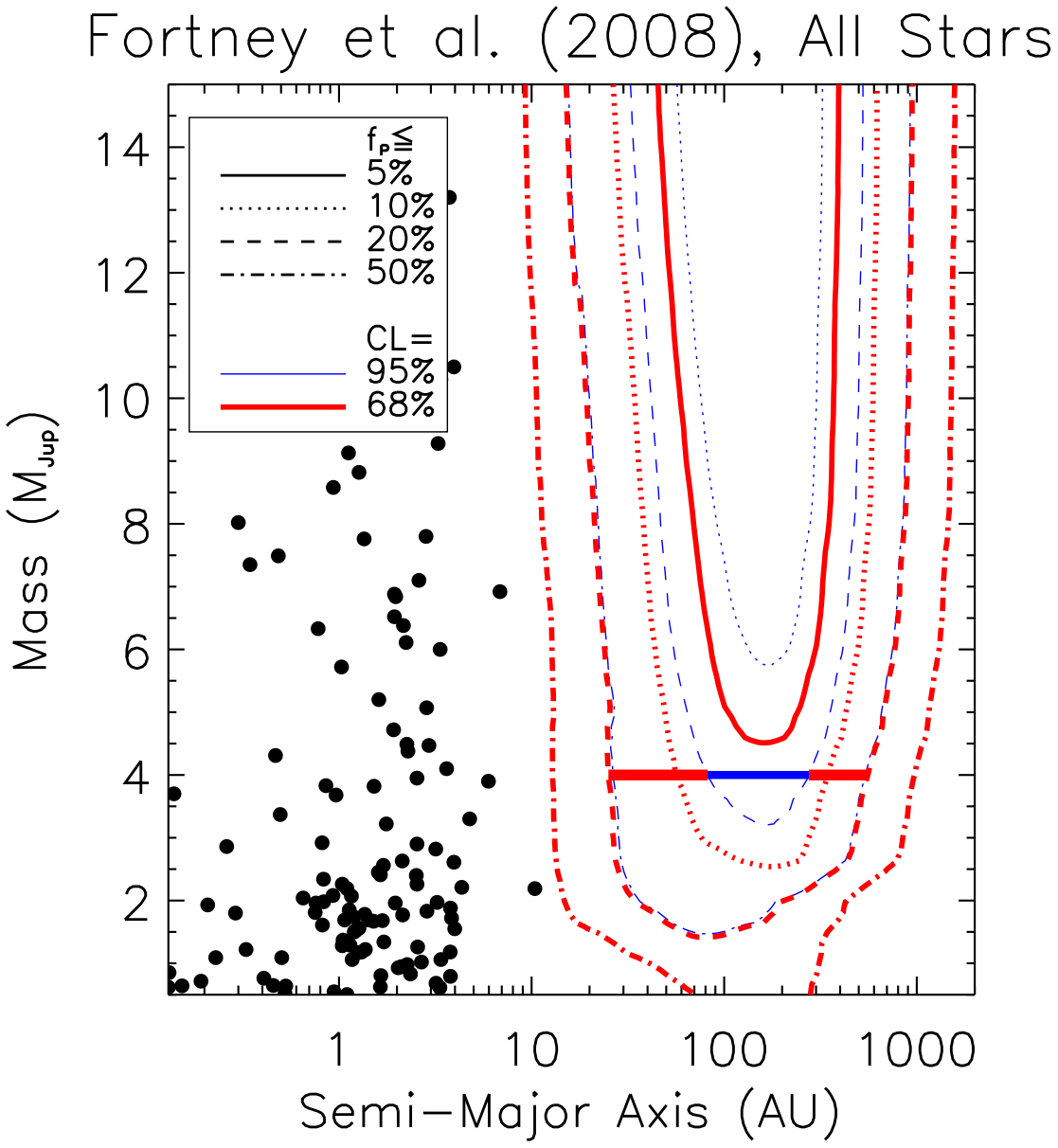

Fig. 6.— The same as Fig. 4 and Fig. 5, this time using the models of Fortney et al. (2008) to give the upper limit on planet fraction. Overall, the theoretical models of Fortney et al. (2008) are more pessimistic as to NIR fluxes of planets when compared to the hot-start models (Burrows et al. 2003; Baraffe et al. 2003). With these models, from 82 to 276 AU, less than 20% of stars can have a planet above 4 M_{Jup}, at the 95% confidence level, and between 25 and 557 AU at 68% confidence.

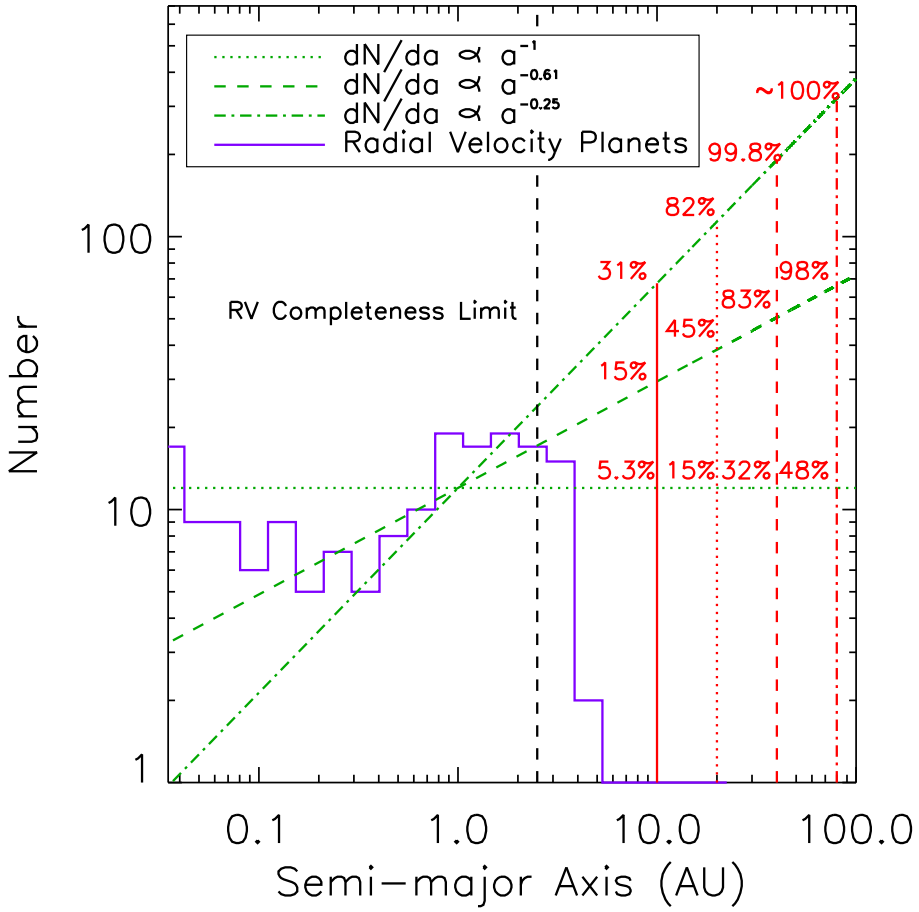

Fig. 7.— Twelve models for the semi-major axis distribution of extrasolar planets, using the planet luminosity models of Baraffe et al. (2003), with power law indices of α = -1, -0.61, and -0.25, and upper cut-offs (the limit up to which there are planets, but beyond which planets no longer appear) of 10, 20, 40, and 80 AU. The solid purple line gives the histogram of known radial velocity planets, the horizontal and diagonal green lines give different values of the power law index, and the red vertical lines mark the upper cut-offs. The vertical black dashed line at 2.5 AU gives the approximate upper limit to which the radial velocity survey is complete to planets. The percentages at each intersection of power law and upper cut-off show the confidence with which that model ($\frac{dN}{da} \propto a^{\alpha}$ for $a \leq a_{cut-off}$, and $\frac{dN}{da} = 0$ for $a > a_{cut-off}$) can be rejected. For example, a planet population with dN/da $\sim$ a^{-1} and an outer cutoff of 10 AU is ruled out at 5.3% confidence. For the power law of index -0.61 (Cumming et al. 2008), at 95% confidence the upper cut-off must be less than 65 AU, which would fall between the dashed and dot-dashed vertical lines of this graph.

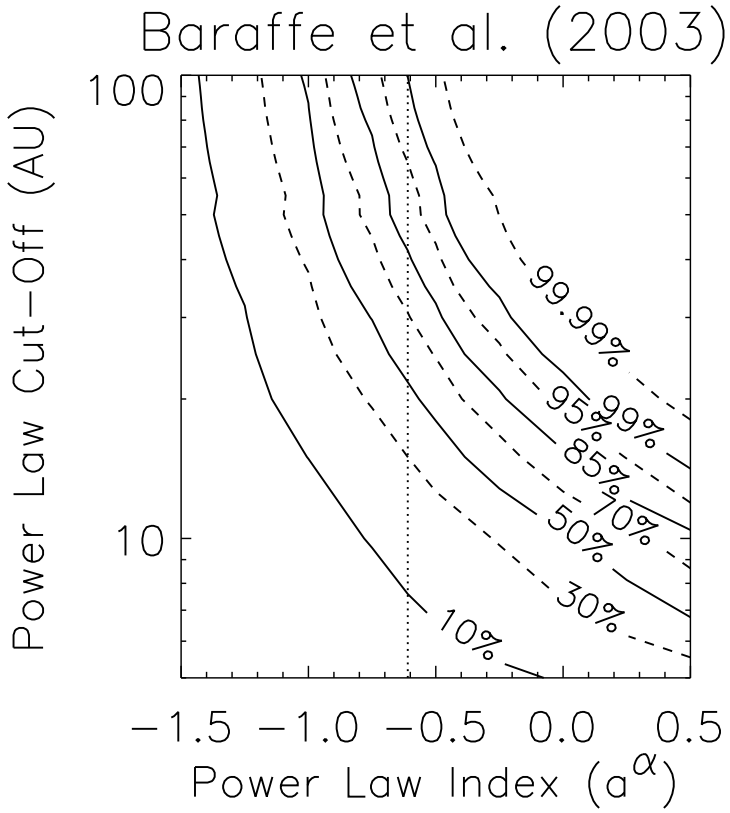

Fig. 8.— Contours showing the confidence with which we can exclude models of the semi-major axis distribution of extrasolar giant planets of the form $\frac{dN}{da} \propto a^{\alpha}$, with an upper cut-off beyond which there are no longer planets, using the models of Baraffe et al. (2003). The power law index of -0.61 as given by Cumming et al. (2008) is marked with a dotted line. The jags in the contours are due to binaries being removed as we move up in power law cut-off (binary target stars are pulled once the considered semi-major axis cut-off reaches one-fifth the binary separation). The pronounced jag between 50 and 55 AU corresponds to the binary M-dwarfs TWA 8A and TWA 8B (21 pc, 10 Myr) being removed from the sample, indicating the strong effect a few M stars have on our results. For the power law of index -0.61, the 68% and 95% confidence levels for rejection of this model are at 30 and 65 AU. Similar plots for the Burrows et al. (2003) and Fortney et al. (2008) models are available in our supplement, available at http://exoplanet.as.arizona.edu/∼lclose/exoplanet2.html , which also contains versions of all future plots for these additional two sets of models. The 68% and 95% confidence levels are 28 and 56 AU (Burrows et al. 2003) and 83 and 182 AU (Fortney et al. 2008).

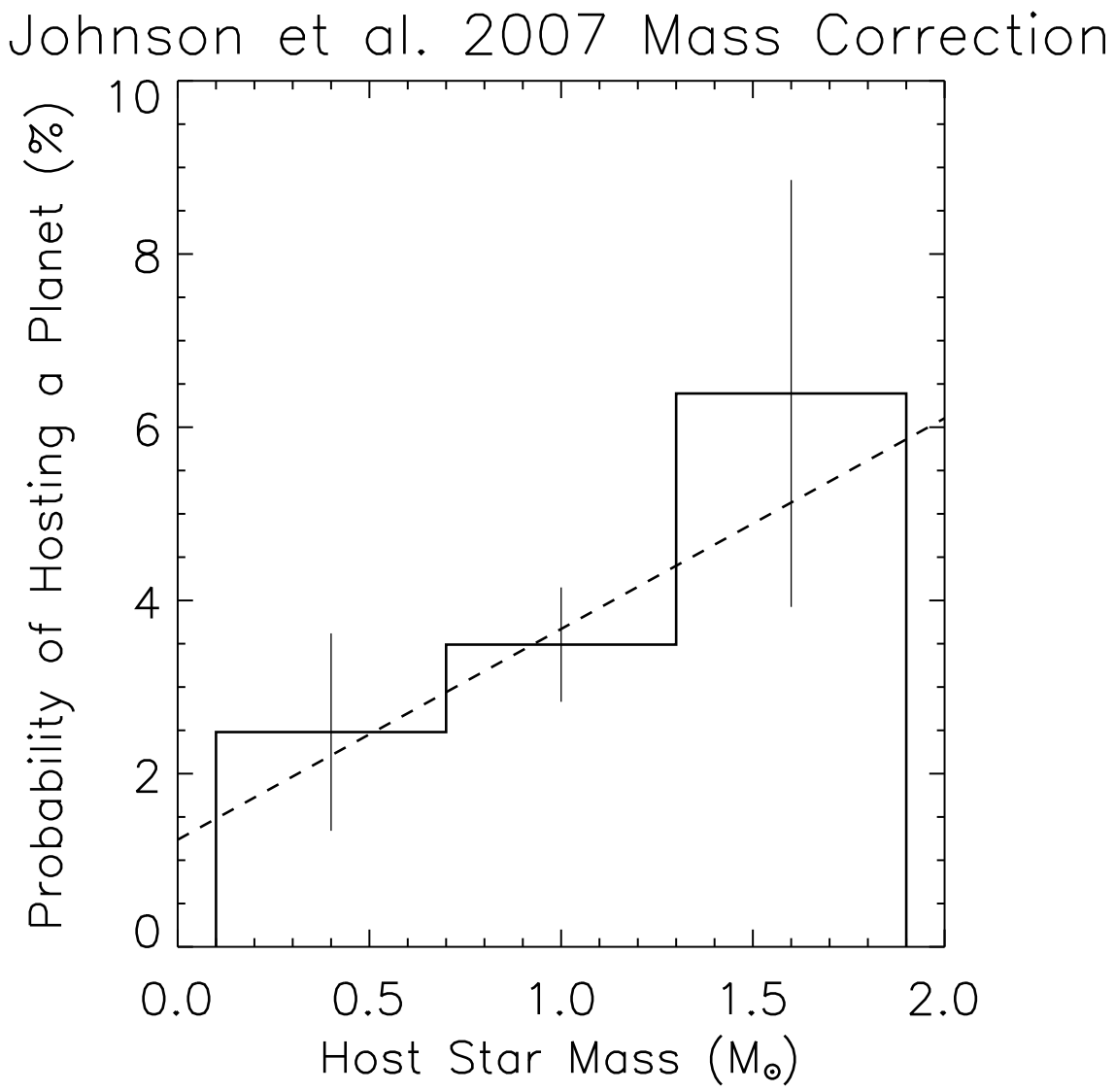

Fig. 9.— Our linear fit to the dependence of the likelihood a target star has of hosting a close-in, giant extrasolar planet as a function of stellar mass. The histogram shown is the metallicity-corrected histogram of Johnson et al. (2007) (their Fig. 6). As noted by Johnson et al. (2007), the probability for the high-mass bin is likely underestimated, so future work may show an even greater boost for the value of high-mass target stars. For the target stars considered in this work, 35 are in the low-mass bin, 78 are in the medium-mass bin, and 5 are in the bin for the highest masses.

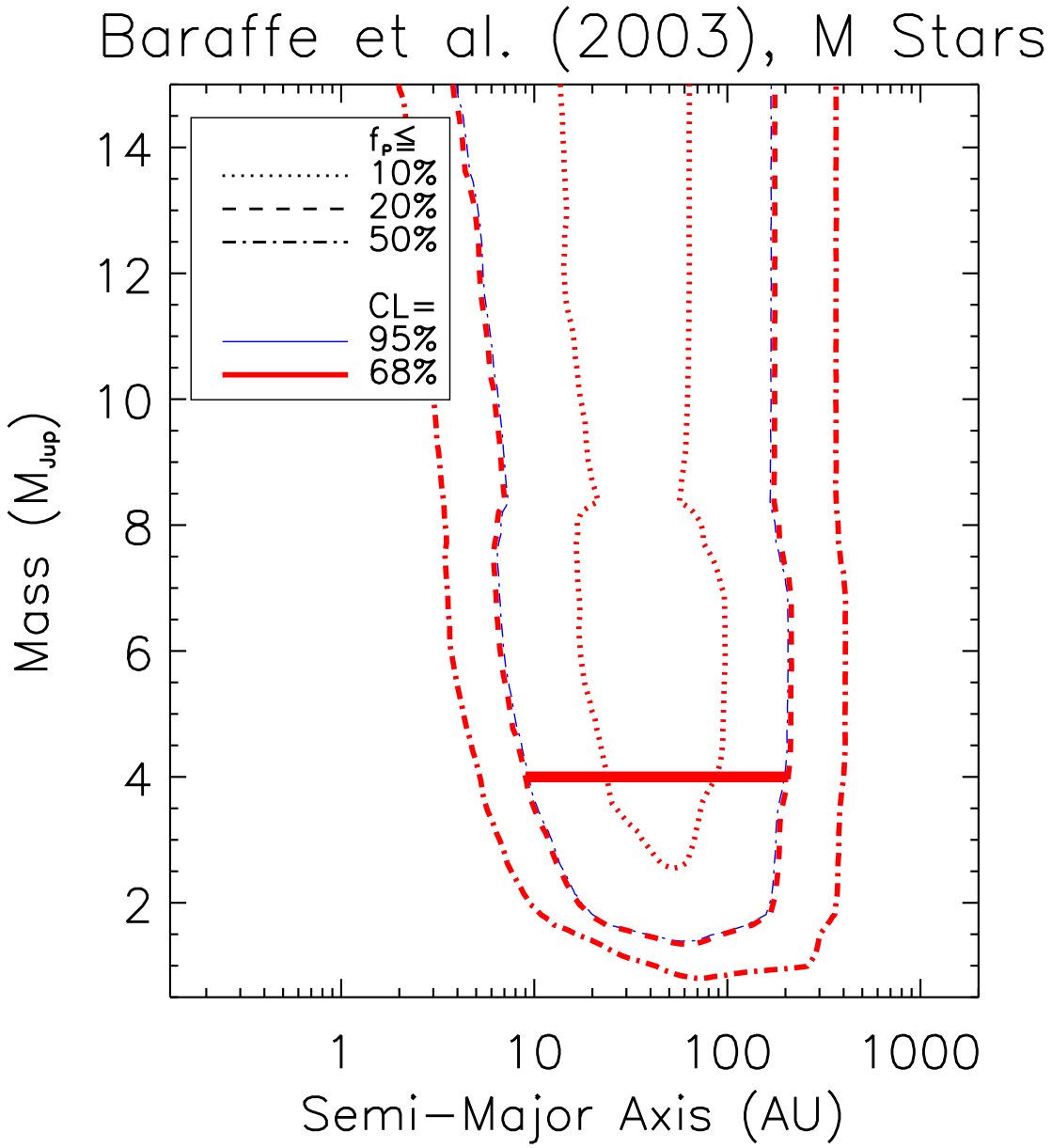

Fig. 10.— Contours giving the upper limit on planet fraction around all the stars of M spectral type in the three surveys, using the models of Baraffe et al. (2003). Comparing to Fig. 4, which considered stars of all spectral types, the behavior of the contours at small semi-major axis is roughly the same, while the outer edge and depth of the upper limit are limited by the reduced sample size (only 18 of the 118 target stars are M stars). For 68% confidence, fewer than 1 in 5 stars have a planet more massive than 4 M_{Jup} between 9.0 and 207 AU. For the models of Burrows et al. (2003) this range is 8.3 to 213 AU, and is 43 to 88 AU for the Fortney et al. (2008) models.

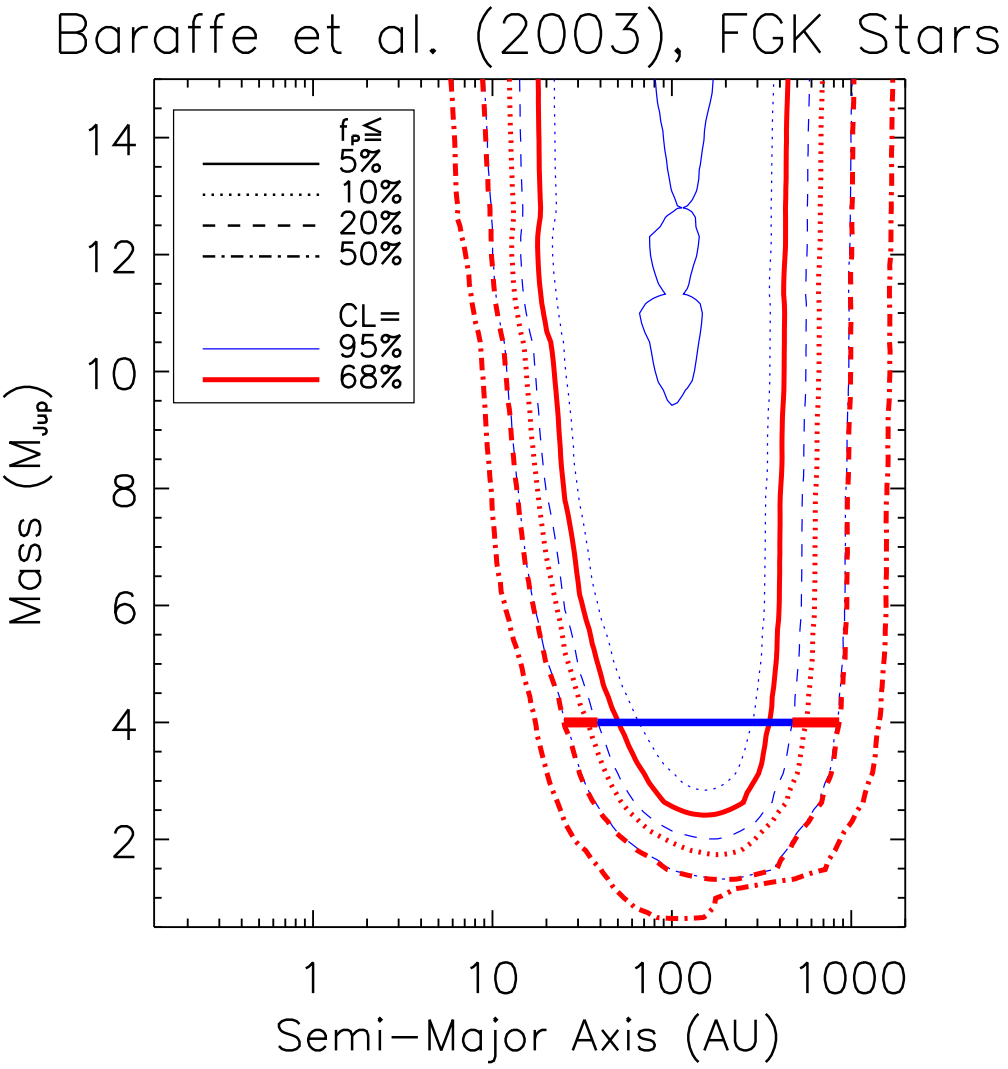

Fig. 11.— The upper limit on planet fraction, using only the FGK stars in our survey (as well as the single A star in the survey, HD 172555 A), using the models of Baraffe et al. (2003). The shapes of the contours and the behavior at large semi-major axes are roughly the same as in Fig. 4, when all stars were considered, but without the M stars and their favorable contrasts at small separations, the small-period planets are much less accessible. The 20% contours, at the 68% and 95% confidence levels, for planets more massive than 4 M_{Jup}, are found between 25 and 856 AU and between 38 and 469 AU, respectively. For the Burrows et al. (2003) models, the 68% and 95% limit ranges are between 25 and 807 AU, and 40 and 440 AU; for the Fortney et al. (2008) models, the 95% confidence 20% contour never reaches 4 M_{Jup}, but the 68% confidence range is from 59 to 497 AU.

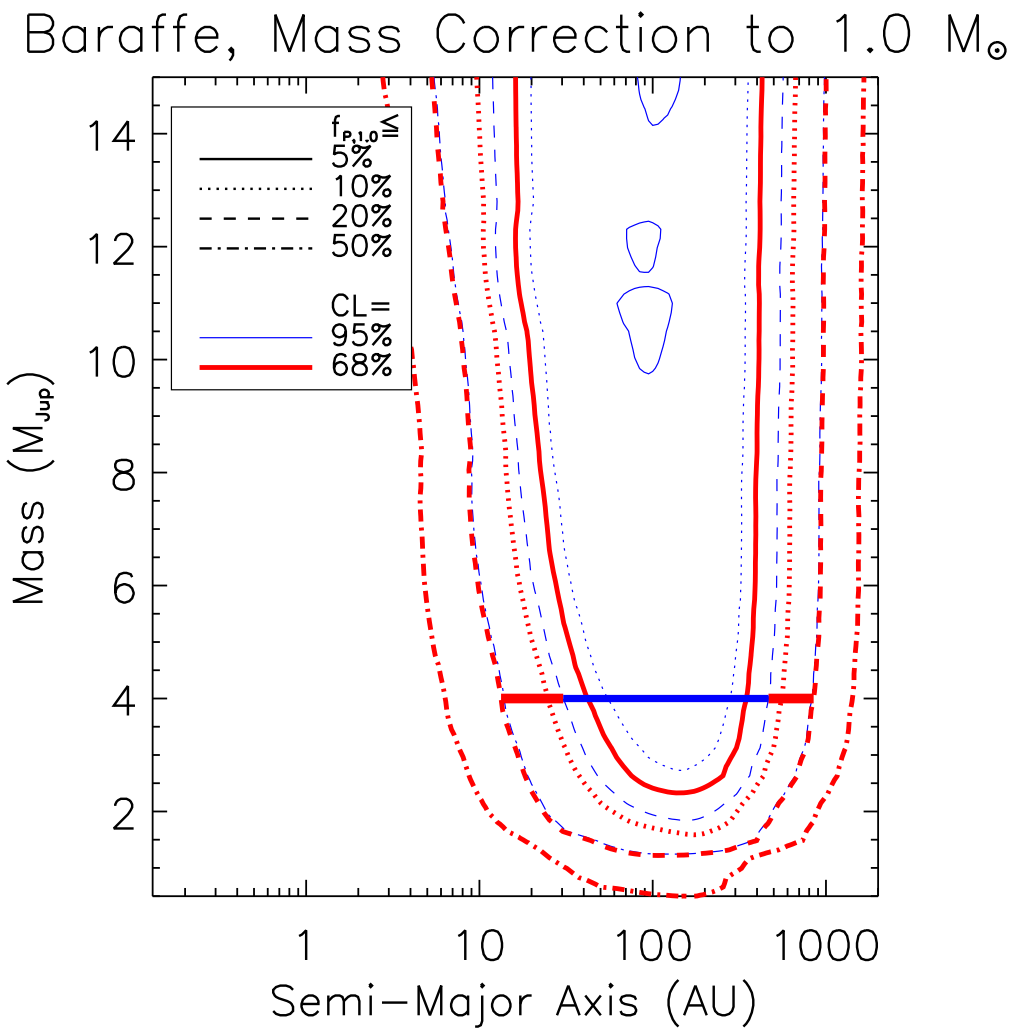

Fig. 12.— The upper limit on planet fraction for stars of 1 $M_{\odot}$ ($f_{p,1.0}$), with constraints from target stars of higher and lower mass stars weighted according to a fit to the Johnson et al. (2007) dependence on stellar mass of the frequency of radial velocity planets, using the models of Burrows et al. (2003). The plot is similar to that of Fig. 4, which weighted all stars equally, but the contours shrink slightly (mainly on the low separation side of the plot) as the M stars are now effectively given less weight. The 20% confidence level for planets more massive than 4 M_{Jup} are between 13 and 849 AU at 68% confidence, and between 30 and 466 AU for the 95% confidence level. For the Burrows et al. (2003) models, these ranges are 13 to 805 AU, and 30 to 440 AU, while for the models of Fortney et al. (2008) the limits are between 41 and 504 AU, and 123 and 218 AU.

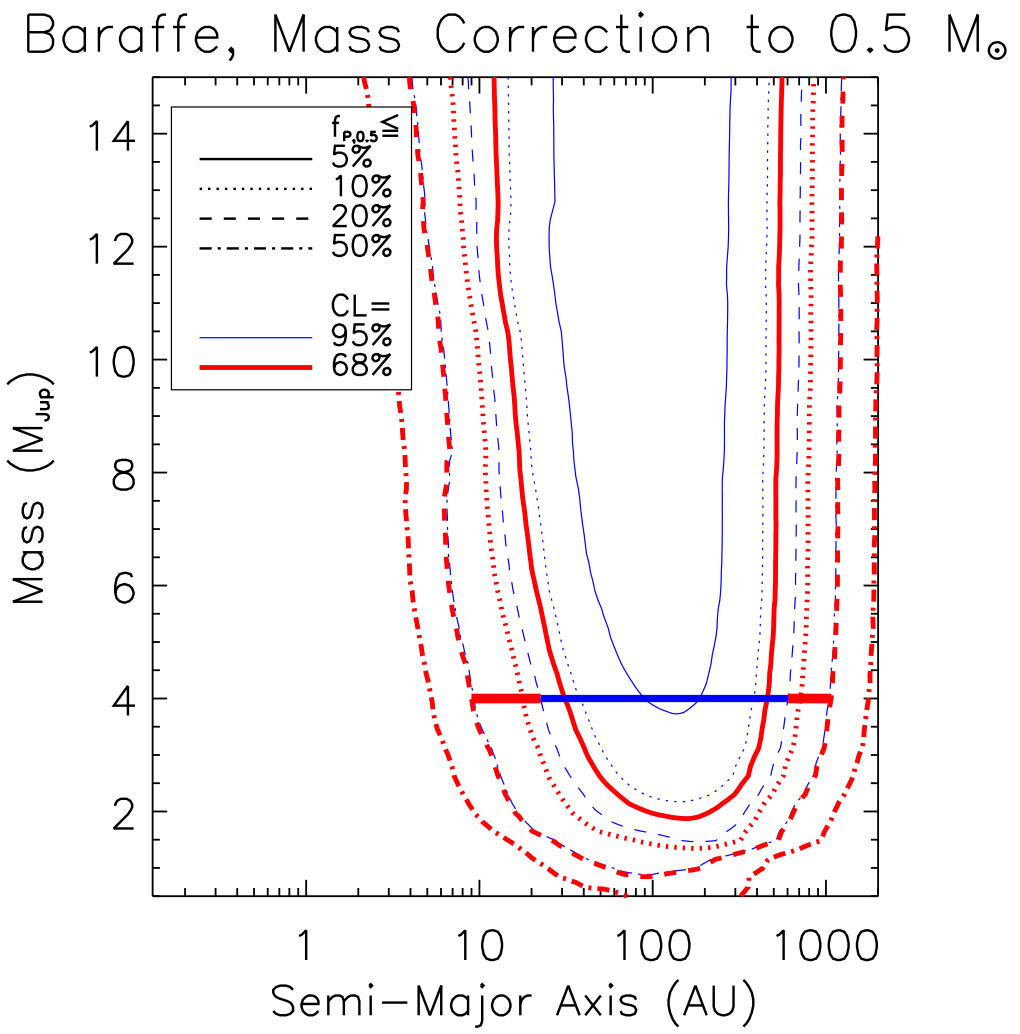

Fig. 13.— The upper limit on planet fraction, this time normalizing to stars of a half solar mass ($f_{p,0.5}$), or about M0, using the models of Baraffe et al. (2003). The constraints become stronger, as expected, as our assumption going into this calculation is that lower mass stars are less likely to have planets overall. With this set of assumptions, the dearth of giant, large-separation planets around M stars is made quite clear. The possibility of lower mass, inner planets around M stars (and indeed, planets like those in our own solar system) remains, however. Fewer than 20% of M stars can have planets more massive than 4 M_{Jup} between 9.0 and 1070 AU at 68% confidence, and 23-605 AU at the 95% confidence level. These limits are 8.3 to 1016 AU and from 22 to 573 AU for the Burrows et al. (2003) models, as well as 26 to 656 AU and 71 to 341 AU for the Fortney et al. (2008).

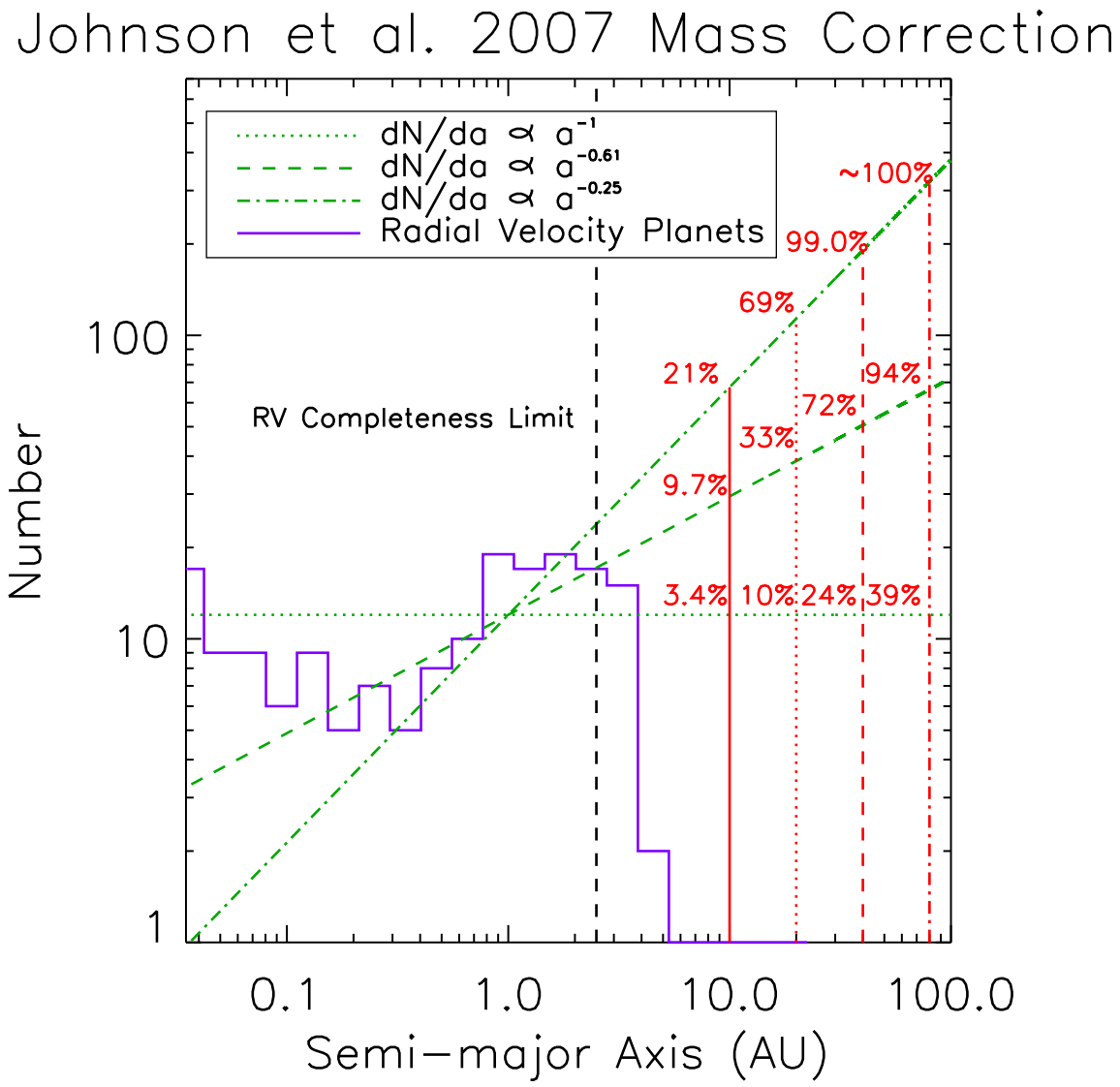

Fig. 14.— As with Fig. 7, power-law models for the semi-major axis distribution of extrasolar planets, and the confidence with which we can rule out these models, using the results of our survey and the models of Baraffe et al. (2003). This time, we utilize the results of Johnson et al. (2007) to appropriately give additional weight to high mass stars, which are more likely to harbor giant planets.

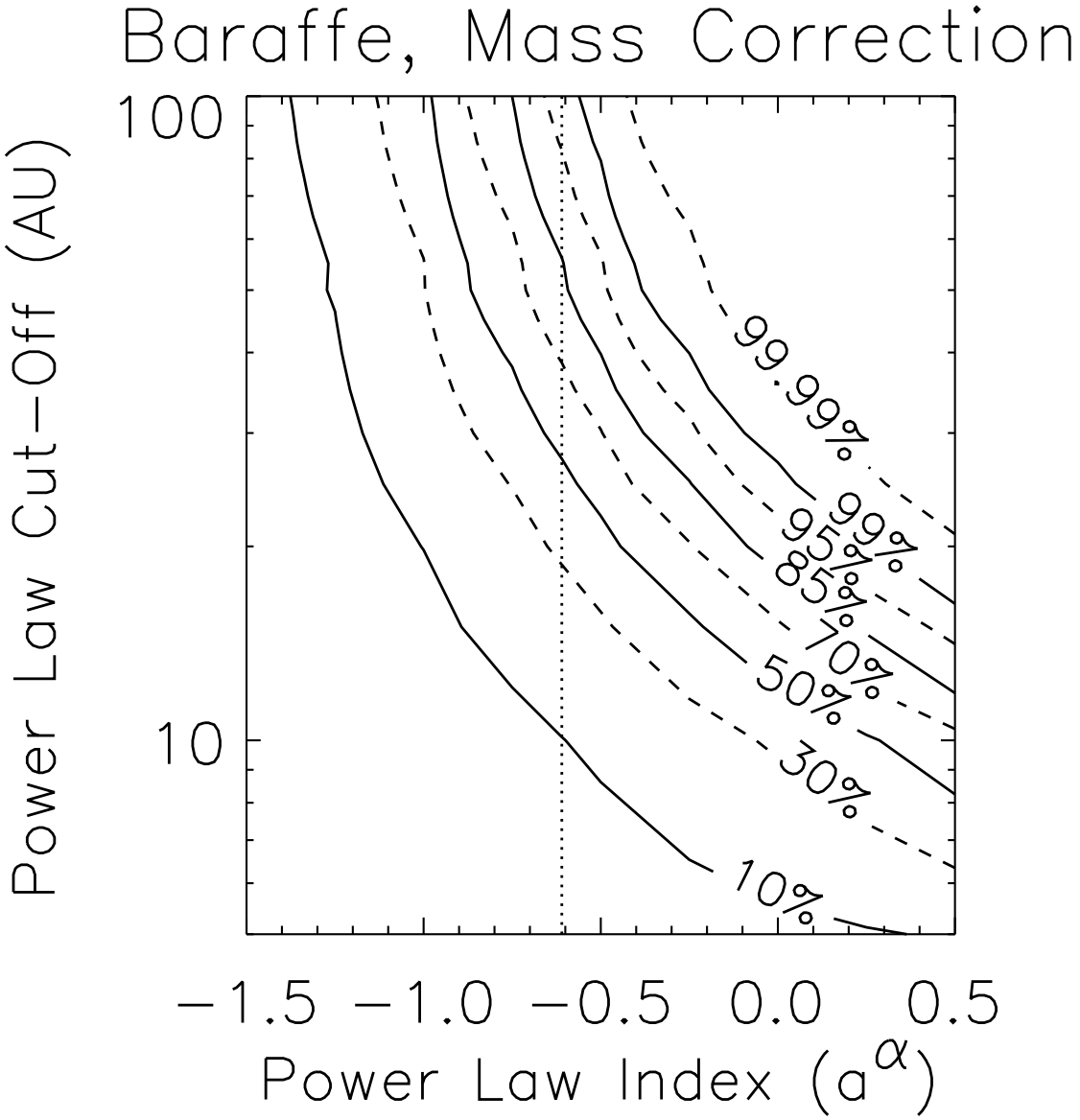

Fig. 15.— Contours showing the confidence with which we can exclude a model for the distribution of semi-major axis of extrasolar giant planets given by $\frac{dN}{da} \propto a^{\alpha}$ up to some upper cut-off. This figure shows the results for the models of Baraffe et al. (2003), with the stellar mass correction of Johnson et al. (2007) to account for the dependence of likelihood of finding giant planets upon the mass of the parent star. The upper cut-off for the Cumming et al. (2008) power law of index -0.61 (as marked by the dotted line) is 37 AU at the 68% confidence level, and 82 at 95% confidence. For the Burrows et al. (2003) models, the 68% and 95% confidence limits are at 36 and 82 AU, and at 104 and 234 AU for the Fortney et al. (2008) models.

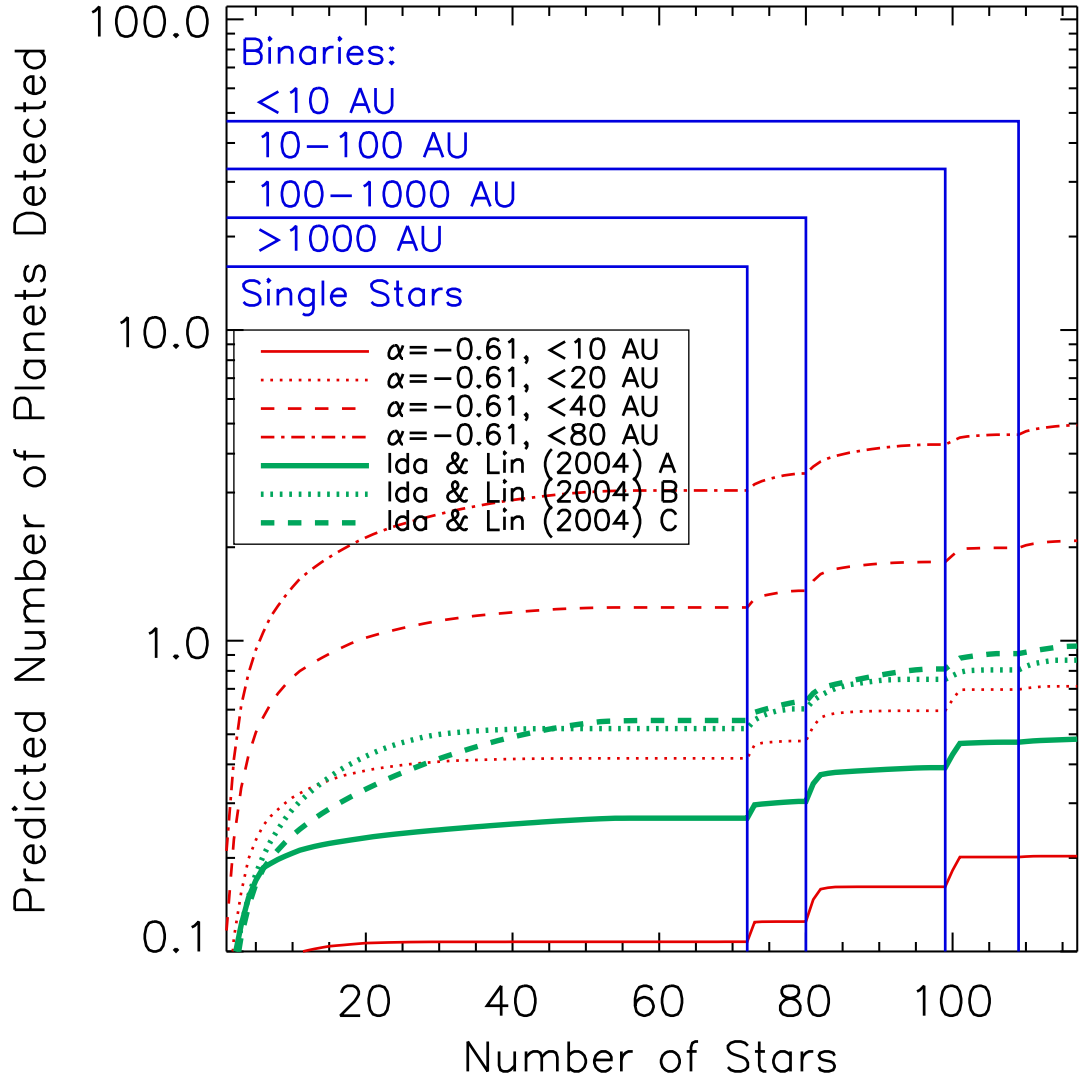

Fig. 16.— The number of planets we'd expect to detect, as a function of the number of stars in our survey. Target stars are divided into bins: one for single stars, and binaries divided by separation; within each bin the best targets are placed to the left of the graph, so they're "observed first" in this manner. Using the models of Baraffe et al. (2003), and not accounting for stellar mass effects or removing binaries, the core accretion models of Ida & Lin (2004) predict detecting between 0.5 and 1 planets with the combination of the Masciadri et al. (2005), Biller et al. (2007), and Lafrenière et al. (2007) surveys. The Ida & Lin (2004) models A, B, and C (green curves) can only be excluded with 38%, 58%, and 62% confidence, respectively.

Table 1. Target Stars

Target	RA[1]	Dec[1]	Distance (pc)[2]	Sp. Type	Age (Myr)	V[1]	H[3]	Ks[3]	Obs. Mode[4]
Biller et al. (2007)									
HIP 1481	00 18 26.1	-63 28 39.0	40.95	F8/G0V	30	7.46	6.25	6.15	VLT SDI
HD 8558	01 23 21.2	-57 28 50.7	49.29	G6V	30	8.54	6.95	6.85	VLT SDI
HD 9054	01 28 08.7	-52 38 19.2	37.15	K1V	30	9.35	6.94	6.83	VLT SDI
HIP 9141	01 57 48.9	-21 54 05.0	42.35	G3/G5V	30	8.11	6.55	6.47	VLT SDI
BD+05 378	02 41 25.9	+05 59 18.4	40.54	M0	12	10.20	7.23	7.07	VLT SDI
HD 17925	02 52 32.1	-12 46 11.0	10.38	K1V	200	6.05	4.23	4.17	VLT SDI/GDPS
Eps Eri	03 32 55.8	-09 27 29.7	3.22	K2V	1100	3.73	1.88	1.78	VLT SDI/GDPS
V577 Per A	03 33 13.5	+46 15 26.5	33.77	G5IV/V	70	8.35	6.46	6.37	MMT SDI
GJ 174	04 41 18.9	+20 54 05.4	13.49	K3V	280	7.98	5.31	5.15	VLT SDI
GJ 182	04 59 34.8	+01 47 00.7	26.67	M1Ve	12	10.10	6.45	6.26	VLT SDI/Ks/GDPS
HIP 23309	05 00 47.1	-57 15 25.5	26.26	M0/1	12	10.09	6.43	6.24	VLT SDI/Ks
AB Dor	05 28 44.8	-65 26 54.9	14.94	K2Vk	70	6.93	4.84	4.69	VLT SDI
UY Pic	05 36 56.8	-47 57 52.9	23.87	K0V	70	7.95	5.93	5.81	VLT SDI
AO Men	06 18 28.2	-72 02 41.4	38.48	K6/7	12	10.99	6.98	6.81	VLT SDI/Ks
HIP 30030	06 19 08.1	-03 26 20.0	52.36	G0V	30	8.00	6.59	6.55	MMT SDI
HIP 30034	06 19 12.9	-58 03 16.0	45.52	K2V	30	9.10	7.09	6.98	VLT SDI
HD 45270	06 22 30.9	-60 13 07.1	23.50	G1V	70	6.50	5.16	5.05	VLT SDI
HD 48189 A	06 38 00.4	-61 32 00.2	21.67	G1/G2V	70	6.15	4.75	4.54	VLT SDI
pi01 UMa	08 39 11.7	+65 01 15.3	14.27	G1.5V	200	5.63	4.28	4.17	MMT SDI/GDPS
HD 81040	09 23 47.1	+20 21 52.0	32.56	G0V	2500	7.74	6.27	6.16	MMT SDI
LQ Hya	09 32 25.6	-11 11 04.7	18.34	K0V	13	7.82	5.60	5.45	MMT/VLT SDI/Ks/GDPS
DX Leo	09 32 43.7	+26 59 18.7	17.75	K0V	200	7.01	5.24	5.12	MMT/VLT SDI/GDPS
HD 92945	10 43 28.3	-29 03 51.4	21.57	K1V	70	7.76	5.77	5.66	VLT SDI/GDPS
GJ 417	11 12 32.4	+35 48 50.7	21.72	G0V	200	6.41	5.02	4.96	MMT SDI/GDPS
TWA 14	11 13 26.5	-45 23 43.0	46.00[5]	M0	10	13.00	8.73	8.49	VLT SDI
TWA 25	12 15 30.8	-39 48 42.0	44.00[5]	M0	10	11.40	7.50	7.31	VLT SDI
RXJ1224.8-7503	12 24 47.3	-75 03 09.4	24.17	K2	16	10.51	7.84	7.71	VLT SDI
HD 114613	13 12 03.2	-37 48 10.9	20.48	G3V	8800	4.85	3.35	3.30	VLT SDI
HD 128311	14 36 00.6	+09 44 47.5	16.57	K0	630	7.51	5.30	5.14	MMT SDI
EK Dra	14 39 00.2	+64 17 30.0	33.94	G0	70	7.60	6.01	5.91	MMT SDI/GDPS
HD 135363	15 07 56.3	+76 12 02.7	29.44	G5V	3	8.72	6.33	6.19	MMT SDI/GDPS
KW Lup	15 45 47.6	-30 20 55.7	40.92	K2V	2	9.37	6.64	6.46	VLT SDI
HD 155555 AB	17 17 25.5	-66 57 04.0	30.03	G5IV	12	7.20	4.91	4.70	VLT SDI/Ks
HD 155555 C	17 17 27.7	-66 57 00.0	30.03	M4.5	12	12.70	7.92	7.63	VLT SDI/Ks
HD 166435	18 09 21.4	+29 57 06.2	25.24	G0	110	6.85	5.39	5.32	MMT SDI
HD 172555 A[6]	18 45 26.9	-64 52 16.5	29.23	A5IV/V	12	4.80	4.25	4.30	VLT SDI
CD -64 1208	18 45 37.0	-64 51 44.6	34.21	K7	12	10.12	6.32	6.10	VLT SDI/Ks
HD 181321	19 21 29.8	-34 59 00.5	20.86	G1/G2V	160	6.48	5.05	4.93	VLT SDI
HD 186704	19 45 57.3	+04 14 54.6	30.26	G0	210	7.03	5.62	5.52	MMT SDI
GJ 799B	20 41 51.1	-32 26 09.0	10.22	M4.5e	12	11.00	5.20	-99.00	VLT SDI/Ks
GJ 799A	20 41 51.2	-32 26 06.6	10.22	M4.5e	12	10.25	5.20	4.94	VLT SDI/Ks
GJ 803	20 45 09.5	-31 20 27.1	9.94	M0Ve	12	8.81	4.83	4.53	VLT SDI/Ks/GDPS
HD 201091	21 06 53.9	+38 44 57.9	3.48	K5Ve	2000	5.21	2.54	2.25	MMT SDI
Eps Indi A	22 03 21.7	-56 47 09.5	3.63	K5Ve	4000	4.69	2.35	2.24	VLT SDI
GJ 862	22 29 15.2	-30 01 06.4	15.45	K5V	6300	7.65	5.28	5.11	VLT SDI

Table 1—Continued

Target	RA[1]	Dec[1]	Distance (pc)[2]	Sp. Type	Age (Myr)	V[1]	H[3]	Ks[3]	Obs. Mode[4]
HIP 112312 A	22 44 57.8	-33 15 01.0	23.61	M4e	12	12.20	7.15	6.93	VLT SDI
HD 224228	23 56 10.7	-39 03 08.4	22.08	K3V	70	8.20	6.01	5.91	VLT SDI
Masciadri et al. (2005)									
HIP 2729	00 34 51.2	-61 54 58	45.91	K5V	30	9.56	6.72	6.53	VLT Ks
BD +2 1729	07 39 23.0	02 11 01	14.87	K7	200	9.82	6.09	5.87	VLT H/GDPS
TWA 6	10 18 28.8	-31 50 02	77.00[5]	K7	10	11.62	8.18	8.04	VLT Ks
BD +1 2447	10 28 55.5	00 50 28	7.23	M2	70	9.63	5.61	5.31	VLT H/GDPS
TWA 8A	11 32 41.5	-26 51 55	21.00[5]	M2	10	12.10	7.66	7.43	VLT Ks
TWA 8B	11 32 41.5	-26 51 55	21.00[5]	M5	10	15.20	9.28	9.01	VLT Ks
TWA 9A	11 48 24.2	-37 28 49	50.33	K5	10	11.26	8.03	7.85	VLT Ks
TWA 9B	11 48 24.2	-37 28 49	50.33	M1	10	14.10	9.38	9.15	VLT Ks
SAO 252852	14 42 28.1	-64 58 43	16.40[7]	K5V	200	8.47	5.69	5.51	VLT H
V343 Nor	15 38 57.6	-57 42 27	39.76	K0V	12	8.14	5.99	5.85	VLT Ks
PZ Tel	18 53 05.9	-50 10 50	49.65	K0Vp	12	8.42	6.49	6.37	VLT Ks
BD-17 6128	20 56 02.7	-17 10 54	47.70	K7	12	10.60	7.25	7.04	VLT Ks
Lafrenière et al. (2007)									
HD 166	00 06 36.7839	+29 01 17.406	13.70	K0V	200	6.13	4.63	4.31	GDPS
HD 691	00 11 22.4380	+30 26 58.470	34.10	K0V	260	7.96	6.26	6.18	GDPS
HD 1405	00 18 20.890	+30 57 22.23	30.60	K2V	70	8.60	6.51	6.39	GDPS
HD 5996	01 02 57.2224	+69 13 37.415	25.80	G5V	440	7.67	5.98	5.90	GDPS
HD 9540	01 33 15.8087	-24 10 40.662	19.50	K0V	2900	6.96	5.27	5.16	GDPS
HD 10008	01 37 35.4661	-06 45 37.525	23.60	G5V	200	7.66	5.90	5.75	GDPS
HD 14802	02 22 32.5468	-23 48 58.774	21.90	G0V	5200	5.19	3.71	3.74	GDPS
HD 16765	02 41 13.9985	-00 41 44.351	21.60	F7IV	290	5.71	4.64	4.51	GDPS
HD 17190	02 46 15.2071	+25 38 59.636	25.70	K1IV	4300	7.81	6.00	5.87	GDPS
HD 17382	02 48 09.1429	+27 04 07.075	22.40	K1V	430	7.62	5.69	5.61	GDPS
HD 18803	03 02 26.0271	+26 36 33.263	21.20	G8V	4400	6.72	5.02	4.95	GDPS
HD 19994	03 12 46.4365	-01 11 45.964	22.40	F8V	6200	5.06	3.77	3.75	GDPS
HD 20367	03 17 40.0461	+31 07 37.372	27.10	G0V	380	6.41	5.12	5.04	GDPS
2E 759	03 20 49.50	-19 16 10.0	27.00	K7V	200	10.26	7.66	7.53	GDPS
HIP 17695	03 47 23.3451	-01 58 19.927	16.30	M3e	70	11.59	7.17	6.93	GDPS
HD 25457	04 02 36.7449	-00 16 08.123	19.20	F5V	70	5.38	4.34	4.18	GDPS
HD 283750	04 36 48.2425	+27 07 55.897	17.90	K2	300	8.42	5.40	5.24	GDPS
HD 30652	04 49 50.4106	+06 57 40.592	8.00	F6V	4500	3.19	1.76	1.60	GDPS
HD 75332	08 50 32.2234	+33 17 06.189	28.70	F7V	270	6.22	5.03	4.96	GDPS
HD 77407	09 03 27.0820	+37 50 27.520	30.10	G0	120	7.10	5.53	5.44	GDPS
HD 78141	09 07 18.0765	+22 52 21.566	21.40	K0	270	7.99	5.92	5.78	GDPS
HD 90905	10 29 42.2296	+01 29 28.025	31.60	G0V	230	6.90	5.60	5.52	GDPS
HD 91901	10 36 30.7915	-13 50 35.817	31.60	K2V	1000	8.75	6.64	6.57	GDPS
HD 93528	10 47 31.1553	-22 20 52.927	34.90	K1V	310	8.36	6.56	6.51	GDPS
HIP 53020	10 50 52.0645	+06 48 29.336	5.60	M4	200	11.66	6.71	6.37	GDPS
HD 96064	11 04 41.4733	-04 13 15.924	24.60	G8V	250	8.41	5.90	5.80	GDPS
HD 102392	11 47 03.8343	-11 49 26.573	24.60	K4.5V	3400	9.05	6.36	6.19	GDPS
HD 105631	12 09 37.2563	+40 15 07.399	24.30	K0V	1500	8.26	5.70	5.60	GDPS
HD 107146	12 19 06.5015	+16 32 53.869	28.50	G2V	190	7.07	5.61	5.54	GDPS
HD 108767 B	12 29 50.908	-16 31 14.99	26.90	K2V	140	8.51	6.37	6.24	GDPS

Table 1—Continued

Target	RA[1]	Dec[1]	Distance (pc)[2]	Sp. Type	Age (Myr)	V[1]	H[3]	Ks[3]	Obs. Mode[4]
HD 109085	12 32 04.2270	-16 11 45.627	18.20	F2V	100	4.31	3.37	3.37	GDPS
BD +60 1417	12 43 33.2724	+60 00 52.656	17.70	K0	270	9.40	7.36	7.29	GDPS
HD 111395	12 48 47.0484	+24 50 24.813	17.20	G5V	1000	6.31	4.70	4.64	GDPS
HD 113449	13 03 49.6555	-05 09 42.524	22.10	K1V	70	7.69	5.67	5.51	GDPS
HD 116956	13 25 45.5321	+56 58 13.776	21.90	G9V	710	7.29	5.48	5.41	GDPS
HD 118100	13 34 43.2057	-08 20 31.333	19.80	K4.5V	280	9.31	6.31	6.12	GDPS
HD 124106	14 11 46.1709	-12 36 42.358	23.10	K1V	1700	7.92	5.95	5.86	GDPS
HD 130004	14 45 24.1821	+13 50 46.734	19.50	K2.5V	5100	7.60	5.67	5.61	GDPS
HD 130322	14 47 32.7269	-00 16 53.314	29.80	KOIII	2900	8.05	6.32	6.23	GDPS
HD 130948	14 50 15.8112	+23 54 42.639	17.90	G2V	420	5.88	4.69	4.46	GDPS
HD 139813	15 29 23.5924	+80 27 00.961	21.70	G5	270	7.31	5.56	5.45	GDPS
HD 141272	15 48 09.4630	+01 34 18.262	21.30	G9V	280	7.44	5.61	5.50	GDPS
HIP 81084	16 33 41.6081	-09 33 11.954	31.93	K9Vkee	70	11.29	7.78	7.55	GDPS
HD 160934	17 38 39.6261	+61 14 16.125	24.54	K7	70	10.18	7.00	6.81	GDPS
HD 166181	18 08 16.030	+29 41 28.12	32.58	G5V	60	7.70	5.61	5.61	GDPS
HD 167605	18 09 55.5001	+69 40 49.788	30.96	K2V	500	8.60	6.45	6.33	GDPS
HD 187748	19 48 15.4478	+59 25 22.446	28.37	G0	140	6.66	5.32	5.26	GDPS
HD 201651	21 06 56.3893	+69 40 28.548	32.84	K0	6800	8.20	6.41	6.34	GDPS
HD 202575	21 16 32.4674	+09 23 37.772	16.17	K3V	700	7.91	5.53	5.39	GDPS
HIP 106231	21 31 01.7137	+23 20 07.374	25.06	K3Vke	70	9.24	6.52	6.38	GDPS
HD 206860	21 44 31.3299	+14 46 18.981	18.39	G0VCH-0.5	200	6.00	4.60	4.56	GDPS
HD 208313	21 54 45.0401	+32 19 42.851	20.32	K2V	6400	7.78	5.68	5.59	GDPS
V383 Lac	22 20 07.0258	+49 30 11.763	10.68	K0	40	8.57	6.58	6.51	GDPS
HD 213845	22 34 41.6369	-20 42 29.577	22.74	F5V	200	5.20	4.27	4.33	GDPS
HIP 114066	23 06 04.8428	+63 55 34.359	24.94	M0	70	10.87	7.17	6.98	GDPS
HD 220140	23 19 26.6320	+79 00 12.666	19.74	K2Vk	85	7.73	5.51	5.40	GDPS
HD 221503	23 32 49.3999	-16 50 44.307	13.95	K6Vk	550	8.60	5.61	5.47	GDPS
HIP 117410	23 48 25.6931	-12 59 14.849	27.06	K5Vke	55	9.57	6.49	6.29	GDPS

[1]from the CDS Simbad service

[2]derived from the Hipparcos survey Perryman et al. (1997)

[3]from the 2MASS Survey Cutri et al. (2003)

[4]In cases where target stars were observed by multiple surveys, the star is listed only in the first section of this table where it appears, either in the Biller et al. (2007) or Masciadri et al. (2005) section, with Observing Mode given as "VLT SDI/Ks" or "VLT H/GDPS," for example.

[5]Distance from Song et al. (2003)

[6]As this is the only star in our sample earlier than F2, we consider this work to be a survey of FGKM stars.

[7]Distance from Zuckerman et al. (2001a)

Table 2. Age Determination for Target Stars

Target	Sp. Type*	Li EW (mas)*	Li Age (Myr)	R'$_{HK}$*	R'$_{HK}$ Age++	Group Membership[1]	Group Age[1]	Adopted Age +++
Biller et al. (2007)								
HIP 1481	F8/G0V[2]	129[3]	100	-4.360[4]	221	Tuc/Hor	30	30
HD 8558	G6V[2]	205[5]	13			Tuc/Hor	30	30
HD 9054	K1V[2]	170[5]	160	-4.236[6]	100	Tuc/Hor	30	30
HIP 9141	G3/G5V[7]	181[8]	13			Tuc/Hor	30	30
BD+05 378	M0[9]					β Pic	12	12
HD 17925	K1V[7]	194[8]	50	-4.357[6]	216	Her/Lyr	200	200
Eps Eri	K2V[10]			-4.598[6]	1129+			1100
V577 Per A	G5IV/V[11]	219[11]	3			AB Dor	70	70
GJ 174	K3V[12]	45[8]	280	-4.066[13]				280
GJ 182	M1Ve[14]	280[15]	12					12
HIP 23309	M0/1[16]	294[16]	12	-3.893[6]		β Pic	12	12
AB Dor	K2Vk[17]	267[8]	10	-3.880[6]	<50	AB Dor	70	70
UY Pic	K0V[18]	263[8]	10	-4.234[6]	78	AB Dor	70	70
AO Men	K6/7[16]	357[16]	6	-3.755[6]		β Pic	12	12
HIP 30030	G0V[19]	219[8]	2			Tuc/Hor	30	30
HIP 30034	K2V[2]					Tuc/Hor	30	30
HD 45270	G1V[2]	149[5]	90	-4.378[6]	254	AB Dor	70	70
HD 48189 A	G1/G2V[2]	145[8]	25	-4.268[6]	105	AB Dor	70	70
pi01 UMa	G1.5V[20]	135[8]	100	-4.400[21]	300			200
HD 81040	G0V[20]	24[22]	2500					2500
LQ Hya	K0V[20]	247[8]	13					13
DX Leo	K0V[20]	180[8]	100	-4.234[6]	78	Her/Lyr	200	200
HD 92945	K1V[20]	138[8]	160	-4.393[6]	285	AB Dor	70	70
GJ 417	G0V[23]	76[24]	250	-4.368[13]	235	Her/Lyr	200	200
TWA 14	M0[25]	600[25]	8			TW Hya	10	10
TWA 25	M0[9]	494[26]	10			TW Hya	10	10
RXJ1224.8-7503	K2[27]	250[27]	16					16
HD 114613	G3V[28]	100[29]	400	-5.118[6]	7900			8800
HD 128311	K0[20]			-4.489[13]	565			630
EK Dra	G0[30]	212[8]	2	-4.106[13]	<50	AB Dor	70	70
HD 135363	G5V[20]	220[8]	3					3
KW Lup	K2V[28]	430[31]	2					2
HD 155555 AB	G5IV[16]	205[8]	6	-3.965[6]	<50	β Pic	12	12
HD 155555 C	M4.5[16]					β Pic	12	12
HD 166435	G0[32]			-4.270[21]	107			110
HD 172555 A	A5IV/V[2]					β Pic	12	12
CD -64 1208	K7[16]	580[16]	5			β Pic	12	12
HD 181321	G1/G2V[28]	131[8]	79	-4.372[6]	243			160
HD 186704	G0[33]			-4.350[21]	205			210
GJ 799B	M4.5e[34]					β Pic	12	12
GJ 799A	M4.5e[34]					β Pic	12	12
GJ 803	M0Ve[34]	51[8]	30			β Pic	12	12
HD 201091	K5Ve[34]			-4.704[13]	2029+			2000
Eps Indi A	K5Ve[34]			-4.851[6]	3964+			4000
GJ 862	K5V[34]			-4.983[6]	6280+			6300

Table 2—Continued

Target	Sp. Type*	Li EW (mas)*	Li Age (Myr)	R'$_{HK}$*	R'$_{HK}$ Age++	Group Membership[1]	Group Age[1]	Adopted Age +++
HIP 112312 A	M4e[9]					β Pic	12	12
HD 224228	K3V[28]	53[8]	630	-4.468[6]		AB Dor	70	70
Masciadri et al. (2005)								
HIP 2729	K5V[2]					Tuc/Hor	30	30
BD +2 1729	K7[20]					Her/Lyr	200	200
TWA 6	K7[35]	560[35]	3			TW Hya	10	10
BD +1 2447	M2[36]					AB Dor	70	70
TWA 8A	M2[35]	530[35]	3			TW Hya	10	10
TWA 8B	M5[35]	560[35]	3			TW Hya	10	10
TWA 9A	K5[35]	460[35]	3			TW Hya	10	10
TWA 9B	M1[35]	480[35]	3			TW Hya	10	10
SAO 252852	K5V[37]					Her/Lyr	200	200
V343 Nor	K0V[2]	300[29]	5	-4.159[6]	40	β Pic	12	12
PZ Tel	K0Vp[18]	267[38]	20	-3.780[4]	<50	β Pic	12	12
BD-17 6128	K7[39]	400[40]	3			β Pic	12	12
Lafrenière et al. (2007)								
HD 166	K0V[41]	74[42]	290	-4.458[13]	460	Her/Lyr	200	200
HD 691	K0V[43]	110[8]	260	-4.380[21]	260			260
HD 1405	K2V[44]	271[45]				AB Dor	70	70
HD 5996	G5V[46]			-4.454[13]	440			440
HD 9540	K0V[7]			-4.774[6]	2900			2900
HD 10008	G5V[47]	103[48]	280	-4.530[13]	740	Her/Lyr	200	200
HD 14802	G0V[17]	51[49]	4000	-4.985[6]	6300			5200
HD 16765	F7IV[50]	73[14]	270	-4.400[13]	300			290
HD 17190	K1IV[51]			-4.870[21]	4300			4300
HD 17382	K1V[51]			-4.450[21]	430			430
HD 18803	G8V[52]			-4.880[21]	4400			4400
HD 19994	F8V[53]	12[54]	8000	-4.880[21]	4400			6200
HD 20367	G0V[55]	113[8]	150	-4.500[21]	610			380
2E 759	K7V[56]	63[57]	260			Her/Lyr	200	200
HIP 17695	M3e[58]					AB Dor	70	70
HD 25457	F5V[59]	91[60]	80	-4.390[21]	280	AB Dor	70	70
HD 283750	K2[61]	33[8]	300	-4.057[13]				300
HD 30652	F6V[62]	15[14]	7500	-4.650[21]	1500			4500
HD 75332	F7V[50]	125[8]	50	-4.470[21]	500			270
HD 77407	G0[63]	162[45]	50	-4.340[21]	190			120
HD 78141	K0[64]	107[8]	270					270
HD 90905	G0V[65]	136[8]	80	-4.430[21]	370			230
HD 91901	K2V[7]	7[66]	1000					1000
HD 93528	K1V[17]	100[8]	260	-4.424[6]	360			310
HIP 53020	M4[67]					Her/Lyr	200	200
HD 96064	G8V[68]	114[8]	250	-4.373[13]	250			250
HD 102392	K4.5V[17]			-4.811[6]	3400+			3400
HD 105631	K0V[69]			-4.650[21]	1500			1500
HD 107146	G2V[70]	125[8]	180	-4.340[21]	190			190
HD 108767 B	K2V[71]	175[72]	140					140

Table 2—Continued

Target	Sp. Type*	Li EW (mas)*	Li Age (Myr)	R'$_{HK}$*	R'$_{HK}$ Age++	Group Membership[1]	Group Age[1]	Adopted Age +++
HD 109085	F2V[17]	37[73]	100					100
BD +60 1417	K0[74]	96[8]	270					270
HD 111395	G5V[52]			-4.580[21]	1000			1000
HD 113449	K1V[17]	142[8]	200	-4.340[13]	190	AB Dor	70	70
HD 116956	G9V[68]	31[24]	1000	-4.447[13]	420			710
HD 118100	K4.5V[68]	25[15]	280	-4.090[13]				280
HD 124106	K1V[17]			-4.675[6]	1700			1700
HD 130004	K2.5V[68]			-4.919[13]	5100$^+$			5100
HD 130322	KOIII[75]			-4.780[21]	2900			2900
HD 130948	G2V[52]	116[8]	230	-4.500[21]	610			420
HD 139813	G5[76]	119[8]	230	-4.400[21]	300			270
HD 141272	G9V[68]			-4.390[21]	280			280
HIP 81084	K9Vkee[77]			-4.210[6]		AB Dor	70	70
HD 160934	K7[78]	40[79]	280			AB Dor	70	70
HD 166181	G5V[80]	186[8]	60					60
HD 167605	K2V[81]	14[57]	500					500
HD 187748	G0[63]	114[8]	140					140
HD 201651	K0[47]			-5.010[21]	6800			6800
HD 202575	K3V[68]			-4.522[13]	700$^+$			700
HIP 106231	K3Vke[68]	140[8]	180	-3.906[13]		AB Dor	70	70
HD 206860	G0VCH-0.5[17]	110[82]	190	-4.400[6]	300	Her/Lyr	200	200
HD 208313	K2V[68]			-4.987[13]	6400$^+$			6400
V383 Lac	K0[83]	259[8]	40					40
HD 213845	F5V[17]			-4.547[6]	830	Her/Lyr	200	200
HIP 114066	M0[78]					AB Dor	70	70
HD 220140	K2Vk[68]	218[8]	85	-4.074[13]				85
HD 221503	K6Vk[17]			-4.486[6]	550$^+$			550
HIP 117410	K5Vke[17]			-4.194[6]	55$^+$			55

[1]Group Membership for TWA, β Pic, Tuc/Hor, and AB Dor from Zuckerman & Song (2004), Her/Lyr from López-Santiago et al. (2006). Group Ages from Zuckerman & Song (2004) (TWA, β Pic, and Tuc/Hor), Nielsen et al. (2005) (AB Dor), and López-Santiago et al. (2006) (Her/Lyr)

*Measurement References: 2: Houk & Cowley (1975), 3: Waite et al. (2005), 4: Henry et al. (1996), 5: Torres et al. (2000), 6: Gray et al. (2006a), 7: Houk & Smith-Moore (1988), 8: Wichmann et al. (2003), 9: Zuckerman & Song (2004), 10: Cowley et al. (1967), 11: Christian & Mathioudakis (2002), 12: Leaton & Pagel (1960), 13: Gray et al. (2003a), 14: Favata et al. (1995), 15: Favata et al. (1997), 16: Zuckerman et al. (2001a), 17: Gray et al. (2006b), 18: Houk (1978), 19: Cutispoto et al. (1995), 20: Montes et al. (2001b), 21: Wright et al. (2004), 22: Sozzetti et al. (2006), 23: Bidelman (1951), 24: Gaidos et al. (2000), 25: Zuckerman et al. (2001b), 26: Song et al. (2003), 27: Alcala et al. (1995), 28: Houk (1982), 29: Randich et al. (1993), 30: Gliese & Jahreiß (1979), 31: Neuhauser & Brandner (1998), 32: Eggen (1996), 33: Abt (1985), 34: Gliese & Jahreiss (1991), 35: Webb et al. (1999), 36: Vyssotsky et al. (1946), 37: Evans (1961), 38: Soderblom et al. (1998), 39: Nesterov et al. (1995), 40: Mathioudakis et al. (1995), 41: Rufener & Bartholdi (1982), 42: Zboril et al. (1997), 43: Eggen (1962), 44: Ambruster et al. (1998), 45: Montes et al. (2001a), 46: Helmer et al. (1983), 47: Perryman et al. (1997), 48: López-Santiago et al. (2006), 49: Pasquini et al. (1994), 50: Cowley (1976), 51: Heard (1956), 52: Harlan & Taylor (1970b), 53: Herbig & Spalding (1955), 54: Israelian et al. (2004), 55: Sato & Kuji (1990), 56: Fleming et al. (1989), 57: Favata et al. (1993), 58: Appenzeller et al. (1998), 59: Malaroda (1975), 60: Lambert & Reddy (2004), 61: Oswalt et al. (1988), 62: Morgan & Keenan (1973), 63: Perry (1969), 64: Schwope et al. (2000), 65: Harlan (1974), 66: Strassmeier et al. (2000), 67: Bidelman (1985), 68: Gray et al. (2003b), 69: Schild (1973), 70: Harlan & Taylor (1970a), 71: Mora et al. (2001), 72: Pallavicini et al. (1992), 73: Mallik et al. (2003), 74: Roeser & Bastian (1988), 75: Upgren & Staron (1970), 76: Pye et al. (1995), 77: Fan et al. (2006), 78: Reid et al.

(1995), 79: Zuckerman et al. (2004), 80: Eggen (1964), 81: Stocke et al. (1991), 82: Chen et al. (2001), 83: Bowyer et al. (1996)

$^{+}$In general, we have only determined Ca R'$_{HK}$ ages for stars with spectral types K1 or earlier, but in the case of these K2-K6 stars, we have only the R'$_{HK}$ measurement on which to rely for age determination. The calibration of Mt. Wilson S-index to R'$_{HK}$ for K5 stars (B-V $\sim$ 1.1 mag) has not been well-defined (Noyes et al. (1984); specifically the photospheric subtraction), and hence applying a R'$_{HK}$ vs. age relation for K5 stars is unlikely to yield accurate ages.

$^{++}$Using Eq. 3 of Mamajek & Hillenbrand (2008) to convert R'$_{HK}$ into age

$^{+++}$In general, ages derived from lithium and/or calcium alone are likely accurate to within a factor of $\sim$2

Table 3. Summary of Results.

Target Stars	Mass Correction*	Confidence Level	Baraffe et al. (2003)	Burrows et al. (2003)	Fortney et al. (2008)
Completeness plots: semi-major axis range with $f_p < 20\%$ for $M > 4\ M_{Jup}$					
All	None	68%	8.1 - 911 AU	7.4 - 863 AU	25 - 557 AU
All	None	95%	22 - 507 AU	21 - 479 AU	82 - 276 AU
M stars	None	68%	9.0 - 207 AU	8.3 - 213 AU	43 - 88 AU
M stars	None	95%	–	–	–
FGK stars	None	68%	25 - 856 AU	25 - 807 AU	59 - 497 AU
FGK stars	None	95%	38 - 469 AU	40 - 440 AU	–
All	1 $M_\odot$	68%	13 - 849 AU	13 - 805 AU	41 - 504 AU
All	1 $M_\odot$	95%	30 - 466 AU	30 - 440 AU	123 - 218 AU
All	0.5 $M_\odot$	68%	9.0 - 1070 AU	8.3 - 1016 AU	26 - 656 AU
All	0.5 $M_\odot$	95%	23 - 605 AU	22 - 573 AU	71 - 341 AU
Upper cut-off on power law distribution for semi-major axis with index -0.61					
All	None	68%	30 AU	28 AU	83 AU
All	None	95%	65 AU	56 AU	182 AU
All	Yes	68%	37 AU	36 AU	104 AU
All	Yes	95%	82 AU	82 AU	234 AU

*The "Mass Correction" column refers to whether or not the Johnson et al. (2007) result, that more massive stars are more likely to harbor giant planets, is used to weight the target stars by stellar mass. For the completeness plots, this correction is either not applied (None) or set to a specific stellar mass, to determine the upper limit on the frequency of giant planets around stars of that mass. For the limits on the upper cut-off on power law distributions, the correction is either applied (Yes) or not (None).

Table 4. Binaries

Target	Sep (“)[1]	Sep. (AU)[1]	Reference	Companion Type
Biller et al. (2007)				
HIP 9141	0.15	6.38	Biller et al. (2007)	mid-G
V577 Per A	7	230	Pounds et al. (1993)	M0
AB Dor	9 (Ba/Bb)	134 (Ba/Bb)	Close et al. (2005)	Binary M stars
AB Dor	0.15 (C)	2.24 (C)	Close et al. (2005)	Very low-mass M Star
HIP 30034	5.5	250	Chauvin et al. (2005)	Planet/Brown Dwarf
HD 48189 A	0.76 (B)	16.5	Fabricius & Makarov (2000)	K star
HD 48189 A	0.14	3.03	Biller et al. (2007)	K star
DX Leo	65	1200	Lowrance et al. (2005)	M5.5
EK Dra	SB	SB	Metchev & Hillenbrand (2004)	M2
HD 135363	0.26	7.65	Biller et al. (2007)	late K/early M
HD 155555 AB	SB (AB)	SB (AB)	Bennett et al. (1967)	G5 and K0 SB
HD 155555 AB	18 (C)	1060 (C)	Zuckerman et al. (2001a)	Target Star 155555 C, M4.5
HD 172555 A	71	2100	Simon & Drake (1993)	Target Star CD -64 1208, K7
HD 186704	13	380	Aitken & Doolittle (1932)	early M
GJ 799A	3.6	36	Wilson (1954)	Target Star GJ 799B, M4.5
HD 201091	16	55	Baize (1950)	K5
Eps Indi A	400	1500	McCaughrean et al. (2004)	Binary Brown Dwarf
HIP 112312	100	2400	Song et al. (2002)	M4.5
Masciadri et al. (2005)				
TWA 8A	13	270	Jayawardhana et al. (1999)	Target Star TWA 8B, M5
TWA 9A	9	576	Jayawardhana et al. (1999)	Target Star TWA 9B, M1
SAO 252852	15.7	260	Poveda et al. (1994)	HD 128898, Ap
V343 Nor	10	432	Song et al. (2003)	M4.5
BD-17 6128	2	100	Neuhäuser et al. (2002)	M2
Lafrenière et al. (2007)				
HD 14802	0.47	10	Lafrenière et al. (2007)	K6
HD 16765	4.14	89	Holden (1977)	∼K
HD 17382	20.3	456	Lépine & Shara (2005)	M4.5
HD 19994	∼5	∼100	Hale (1994)	M3V
HD283750	124	2220	Holberg et al. (2002)	White Dwarf
HD 77407	1.7	50	Mugrauer et al. (2004)	∼M
HD 93528	234	8200	Perryman et al. (1997)	HIP 52776, K4.5[2]
HD 96064	11.47	283 AU	Lippincott & MacDowall (1979)	NLTT 26194, M3
HD 102392	1.13	28	Lafrenière et al. (2007)	∼M
HD 108767 B	23.7	639	Gould & Chanamé (2004)	A0IV
HD 130948	2.64	47	Potter et al. (2002)	Binary brown dwarfs
HD 139813	31.5	683	Stephenson (1960)	G0
HD 141272	17.8	350	Eisenbeiss et al. (2007)	M3
HD 160934	SB	SB	Hormuth et al. (2007)	early M, $a = 4.5$ AU
HD 160934	8.69	213	Lowrance et al. (2005)	∼M
HD 166181	SB	SB	Nadal et al. (1974)	1.8 day orbit
HD 166181	0.102	3	Lafrenière et al. (2007)	∼K
HD 167605	1.2	37	Arribas et al. (1998)	M4V
HD 206860	43.2	795	Luhman et al. (2007b)	T dwarf
HD 213845	6.09	139	Lafrenière et al. (2007)	late M

Table 4—Continued

Target	Sep (“)[1]	Sep. (AU)[1]	Reference	Companion Type
HD 220140	10.9	214	Lowrance et al. (2005)	mid M
HD 220140	963	19000	Makarov et al. (2007)	∼M
HD 221503	339	4700	Gould & Chanamé (2004)	binary M stars
HIP 117410	1.84	50	Rossiter (1955)	early M

[1]SB indicates a spectroscopic binary

[2]These stars have *Hipparcos* proper motion and parallax within errors, and similar values of calcium R'$_{HK}$ (-4.424 and -4.451 for HD 93528 and HIP 52776, respectively).